Bioorganic Chemistry 85 (2019) 515–533

Contents lists available at ScienceDirect

Bioorganic Chemistry

journal homepage: www.elsevier.com/locate/bioorg

Design, synthesis and biological study of hybrid drug candidates of nitric oxide releasing cucurbitacin-inspired estrone analogs for treatment of hepatocellular carcinoma

Mahrous A. Abou-Salim[a,d], Mohamed A. Shaaban[b], Mohammed K. Abd El Hameid[b], Yaseen A.M.M. Elshaier[c], Fathi Halaweish[d,*]

[a] Al-Azhar University, Faculty of Pharmacy, Pharmaceutical Organic Chemistry, Assiut 71524, Egypt
[b] Cairo University, Faculty of Pharmacy, Pharmaceutical Organic Chemistry, Cairo 11562, Egypt
[c] University of Sadat City, Faculty of Pharmacy, Organic and Medicinal Chemistry, Menoufia 32958, Egypt
[d] South Dakota State University, Chemistry & Biochemistry, Box 2202, Brookings, SD 57007, USA

ARTICLE INFO

Keywords:
Nitric oxide
HCC
EGFR
DAF-FM DA
MRP2
MAPK
NO-CIEAs

ABSTRACT

Development of hybrid drug candidates is well known strategy for designing antitumor agents. Herein, a novel class of nitric oxide donating cucurbitacin inspired estrone analogs (NO-CIEAs) were designed and synthesized as multitarget agents. Synthesized analogs were initially evaluated for their *anti*-hepatocellular carcinoma activities. Among the tested analogs, NO-CIEAs **17** and **20a** exhibited more potent activity against HepG2 cells (IC_{50} = 4.69 and 12.5 μM, respectively) than the reference drug Erlotinib (IC_{50} = 25 μM). Interestingly, NO-CIEA **17** exerted also a high potent activity against Erlotinib-resistant HepG2 cell line (HepG2-R) (IC_{50} = 8.21 μM) giving insight about its importance in drug resistance therapy. Intracellular measurements of NO revealed that NO-CIEAs **17** and **20a** showed a significant increase in NO production in tumor cells after 1 h of incubation comparable to the reference prodrug JS-K. Flow cytometric analysis showed that both NO-CIEAs **17** and **20a** mainly arrested the HepG2 cells in the G0/G1 phase. Also, In-Cell Based ELISA screening showed that NO-CIEA **17** resulted in a potential inhibitory activity towards the EGFR and MAPK (25% and 29% inhibition compared to untreated control cells, respectively). This data suggests the binding ability of NO-CIEA **17** to the EGFR and ERK to be well correlated along with the docking and cellular studies. Also, treatment of HepG2-R cells with NO-CIEA **17** showed a potential reduction of MRP2 expression in a dose dependent manner providing a significant impact on the chemotherapeutic resistance. Overall, the current study provides a potential new approach for the discovery of a novel antitumor agent against HCC.

1. Introduction

Hepatocellular Carcinoma (HCC) is the most common primary malignancy of the liver and the third most fatal cancer worldwide since it has high incidence to mortality ratio (1.07) [1,2]. Among all cancers, HCC is one of the fast growing causes of death in the US with a death to survival ratio of 0.72 in 2018 [3,4]. In Egypt, HCC is the second most common cancer in men and the sixth most common cancer in women [5]. It poses a significant economic burden on healthcare [4]. HCC has a multitude of etiological risk factors that have also been associated strongly with its development such as hepatotropic viruses (HBV, HCV, and hepatitis D virus (HDV)), alcoholism, aflatoxin, cirrhosis, autoimmune hepatitis, nonalcoholic steatohepatitis (NASH), hemochromatosis (Iron overload in the body), and type 2 diabetes (probably aided by obesity) [4].

For patients with advanced stage HCC, systemic therapy with epidermal growth factor receptor specific tyrosine kinase inhibitors (EGFR-TKIs) such as Erlotinib (Tarceva®) (Fig. 1) to induce cell cycle arrest and apoptosis and increase chemo sensitivity is recommended [6]. The major problems associated with the available chemotherapeutic agents are drug resistance, which occurs with 30–80% of cancer patients. HCC cells produce drug resistance via three mechanisms: multidrug resistance (MDR), P-glycoprotein drug resistance (P-gp) and multidrug resistance protein (MRP). All of them are activated and effective in the HCC treatment process [7,8]. Therefore, there is an urgent need to design a new active molecular target anti-cancer agent for HCC to overcome the toxicity and cellular resistance problems.

Nitric oxide (NO) is an endogenous short-lived free radical obtained

* Corresponding author.

https://doi.org/10.1016/j.bioorg.2019.01.068
Received 12 September 2018; Received in revised form 27 January 2019; Accepted 30 January 2019
Available online 01 February 2019
0045-2068/

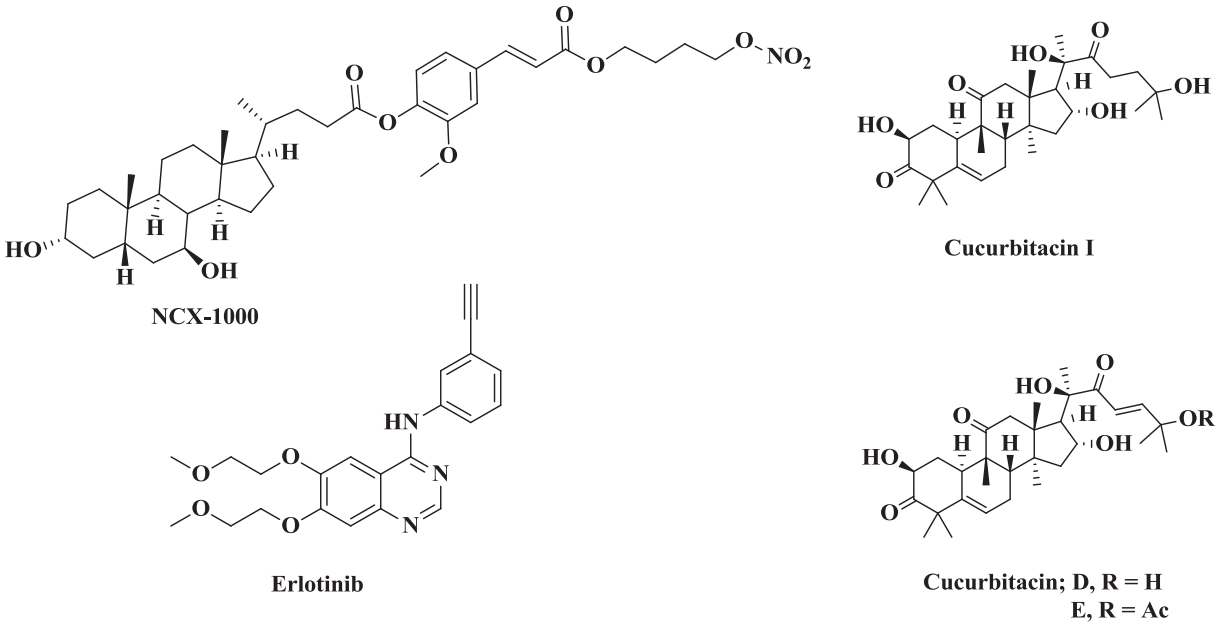

Fig. 1. Structures of NCX-1000, CUCs and current antitumor drugs.

from conversion of L-arginine to L-citroline [9], which is mediated by nitric oxide synthase (NOS) [10]. NO producing compounds have a wide biological function as anticancer agents in addition to their gastrointestinal safety and hepatoprotective properties [9,11–15]. It is also known to reverse chemotherapy resistance in cancer as colon cancer and inhibited the MRP3 efflux pump by nitrating the tyrosine and thereby led to inversion of drug resistance [16–18]. Hence, it is likely that NO can be used in conjunction with traditional cancer drugs that have become ineffective due to such modes of efflux. It is noteworthy to mention that, NCX-1000 (Fig. 1) is the first hepatoprotective NO donor, however, it has not met the endpoint in phase 2 clinical trials [11,19–21].

Cucurbitacin's (CUCs) is highly oxidized tetracyclic triterpenoids isolated from a well-known anticancer family *Cucurbitaceae*. Previous studies on natural or semi-synthetic CUCs in our research group and other scientists demonstrated the ability of several types of CUCs to target EGFR-TK and the whole MAPK signaling pathway using mutant B-Raf cell lines through inhibition of proliferation and induction of apoptosis [22–24]. Among them, cucurbitacin D, E and I (Fig. 1) had a potent in vitro cytotoxic activity against HepG2 cell line and prolonged the survival time, life span and normalizes the biochemical parameters of mice-bearing tumor of Ehrlich's ascites carcinoma [22,25]. CUCs are formed in minute quantities in plants and isolating substantial amounts remain a challenge. Also, the existing methodology available for the total synthesis of these compounds would not be sufficient for the procurement of sufficient quantities for detailed biological evaluation or the synthesis of analogues. Interestingly, CUCs possess an estrone bioisosteric base-scaffold (Fig. 2) and this devoted us to *in silico* design and synthesize estrone analogs-hybrid of CUCs side chain and estrone base-scaffold against EGFR kinase domain [26].

Recently, Korita et al [27] suggested that efficacy of cisplatin-based chemotherapy in patients with HCC depends upon MRP2 expression level [27]. MRP2 is the second member of the MRP subfamily of ABC transporter. The first time MRP2 was cloned from rat hepatocyte and was named as a hepatocellular canalicular multiple organic anion transporter (cMOAT) [28]. In addition, MRP2 shares 49% amino acid identity with MRP1 but it has a different expression pattern. While MRP1 is widely expressed in many tissues, MRP2 is mainly expressed in the apical (canalicular) hepatocyte plasma membrane, small intestine, and renal proximal tubules [29]. Because of the similarity between MRP2 and MARP1, it was believed to confer resistance to similar anticancer drugs too. This hypothesis was created based on an experiment in which an antisense RNA construct was introduced into human HCC HepG2 cells, causing in increased sensitivity to several anticancer drugs such as cisplatin, vinblastine, sorafenib, doxorubicin, and erlotinib [28]. MRP2 has been demonstrated to transport vinblastine in polarized Madin Darby canine kidney epithelial (MDCK) cells, proposing a potential role for MRP2 in resistance. In addition, transfected cells also conferred resistance to cisplatin, etoposide, doxorubicin, and epirubicin. This phenomenon is convincible to suggest a potential role for MRP2 in drug resistance such as erlotinib against HepG2 resistance cell line [30,31].

Enlightened by the aforementioned and on continuation to our previous work [32], we envisioned that tethering NO releasing moiety to CIEAs known of potent inhibition of HCC, will significantly impact the potential anticancer activity of hybrid drug candidate as a result of synergistic effects of NO and CIEA. In this context, we aim to design and synthesize novel hybrid drug candidates of nitric oxide releasing cucurbitacin-inspired estrone analogs (NO-CIEAs) as potential nitric oxide releasing motifs targeting EGFR-ERK signaling pathway for treatment of HCC and overcoming the chemotherapeutic resistance.

2. Design strategy

Modification of ring A of estrone has received substantial attention to block the estrogenic activity of the free phenolic OH group of estrone analogs [33]. So, we envisioned that tethering the C-3 phenolic OH with NO-releasing functionality is expected to have a significant impact on the anticancer activity of CIEAs with dual effect; block the estrogenic effect and site of NO source. Furoxan and organic nitrate moieties were chosen as NO donor source (Fig. 2).

Also, incorporation of various pharmacophores at C-17 of ring D has produced analogs that induce apoptosis in different cancer cell lines [23,24]. Therefore, to investigate further biological activity associated with the C-17 functionalized estrone structure and its side chain, a new set of estrogen derived targets were identified for synthesis of novel hybrid molecules with high binding affinity to molecular targets (Fig. 2).

In this context, we envisioned that a novel drug candidate of hybrid structure (1) the NO donating group appendix on phenolic OH; (2) using estrone base-scaffold as it considered as natural bioisostere to CUCs architecture and finally (3) C-17 functionalization with important

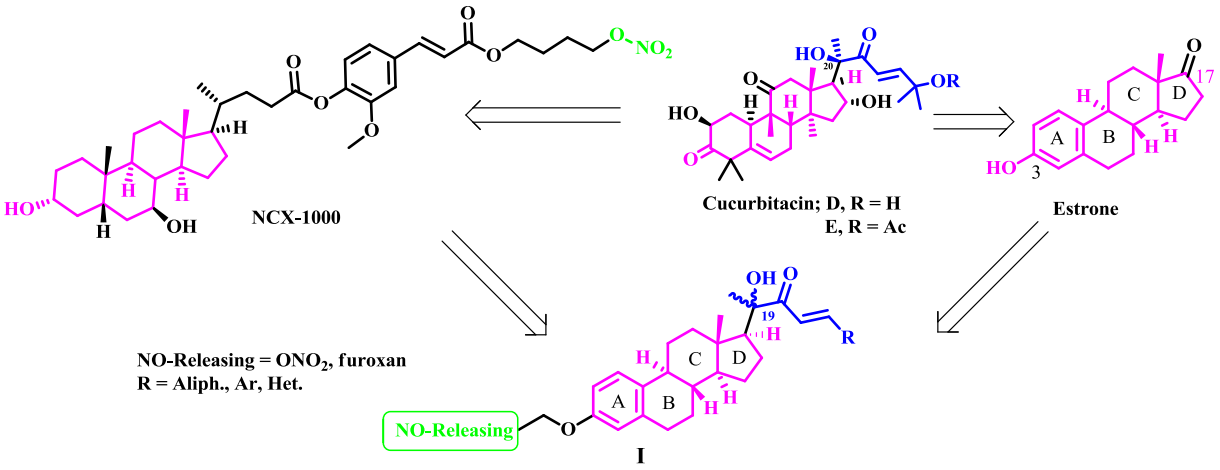

Fig. 2. Design strategy for target compounds NO/CIEA hybrids.

CUCs side chain as well as aryl and heterocyclic substituted α,β-unsaturated ketones assembled to CUCs side chain. The chemical structures were chosen and constructed by utilizing molecular docking for many runs before starting synthetic study. All designed compounds were fully characterized and underwent biological investigations to evaluate their activity for treatment of HCC. Also, this widens our armaments against a devastating disease that we are failing to face.

3. Results and discussion

3.1. In silico molecular modeling

A library of NO-CIEA hybrids was designed and energy minimized using MMFF94 force field calculations. The catalytic domain of two different receptors EGFR (PDB code: 1M17 [34]) and ERK (PDB code: 2OJJ [35]) were downloaded from PDB and prepared for docking using Open Eye® software [34]. Different conformations of each ligand were generated by Open Eye® Omega application. Docking was conducted using Fred® and the data was visualized by Vida® application. Consensus scoring which is a filtering processes to obtain virtual binding affinity will be generated and the lower consensus score, the better binding affinity of the ligands towards the molecular targets. Docking study was operated with multi running time and the best 10 compounds were selected to the next run and then 50–70 compounds were derivatized a library component.

The docking study with EGFR revealed that all the target compounds showed better consensus score than the lead drug Erlotinib, NCX-1000 and CUCs D, E and I, Table 1. To validate our docking method, the standard Erlotinib showed a hydrogen bond (HB = 2.27 Å) towards ATP-binding site of EGFR coming from pyrimidine-N2 with Met:769:A (Fig. 3A). This docking mode and pose similar to co-crystalized docking pose of Erlotinib with receptor [34]. NO-CIEAs **17** (Fig. 3B), **20a,b,g, 23a,b, 30** and NCX-1000 showed only a hydrophobic-hydrophobic interaction towards the ATP binding site of EGFR. Also, NO-CIEA **20f** showed a hydrophobic-hydrophobic interaction towards the ATP binding site as well as a HB between C-19 hydroxyl group (donor) and carbonyl oxygen (acceptor) of Met:769:A with bond length 2.30 Å (Fig. 3C). Furthermore, **20d** and **20e** showed a hydrophobic-hydrophobic interaction towards the ATP binding site as well as a hydrogen bond between Lys:721:A (donor) and carbonyl oxygen of ring D of **20d** (acceptor) and furoxan oxygen of **20e** (acceptor) with bond length 1.56 and 2.11 Å, respectively, while compound **20c** showed a hydrogen bonding between C-19 hydroxyl group (donor) and carbonyl oxygen of Asn:818:A (acceptor) with bond length 1.99 Å. Moreover, as shown in Fig. 3D, there is an overlay of the docking pose of NO-CIEAs **17** (gray) and **20f** (green) in the EGFR active site.

Table 1
Consensus scores of NO/CIEA hybrids and **Erlotinib** and **82A** as reference drugs.

Compound	Consensus score	
	EGFR[c]	ERK[d]
17	36	6
20a	18	68
20b	19	58
20c	29	42
20d	25	56
20e	25	61
20f	7	61
20g	20	41
23a	31	44
23b	34	65
30	21	76
Erlotinib[a]	37	33
CUCs I	44	18
NCX-1000	47	21
CUCs D	59	19
CUCs E	63	21
82A[b]	–	7

[a] EGFR co-crystalized ligand.
[b] ERK1 co-crystalized ligand.
[c] PDB code: 1M17.
[d] PDB code: 2OJJ.

Then, the docking study with ERK kinase domain (PDB code: 2OJJ) [35] revealed that NO-CIEA **17** shows a consensus score better than the co-crystallized ligand (82A; drug bank ID: DB07264) [35], Table 1. The amide carbonyl of the co-crystallized ligand (82A) formed a HB with Lys:52:A. Its pyrazole-linked phenyl showed a hydrophobic interaction with Val:37:A of the glycine-rich loop. Also, the pyrrole NH showed a hydrogen bond with the side chain carbonyl of the gatekeeper residue Gln:103:A (Fig. 4A). This docking mode similar to co-crystalized docking pose with receptor [35]. The data also showed that the furoxan N2-oxygen of NO-CIEA **17** formed a HB (acceptor) with the Lys:52 (donor) (2.41 Å), and the steroidal backbone made a hydrophobic interaction with Val:37 of the glycine-rich loop. Also, the furoxan N4 was involved in a HB (acceptor) with the phenolic OH of Tyr:34:A (donor) with bond length 2.07 Å (Fig. 4B).

3.2. Chemistry

The synthetic pathway of the key intermediate α-hydroxy methyl ketones (**7a,b**) is summarized in Scheme 1. To install the C-17 side chain, the synthetic route was started with protection of the C-3

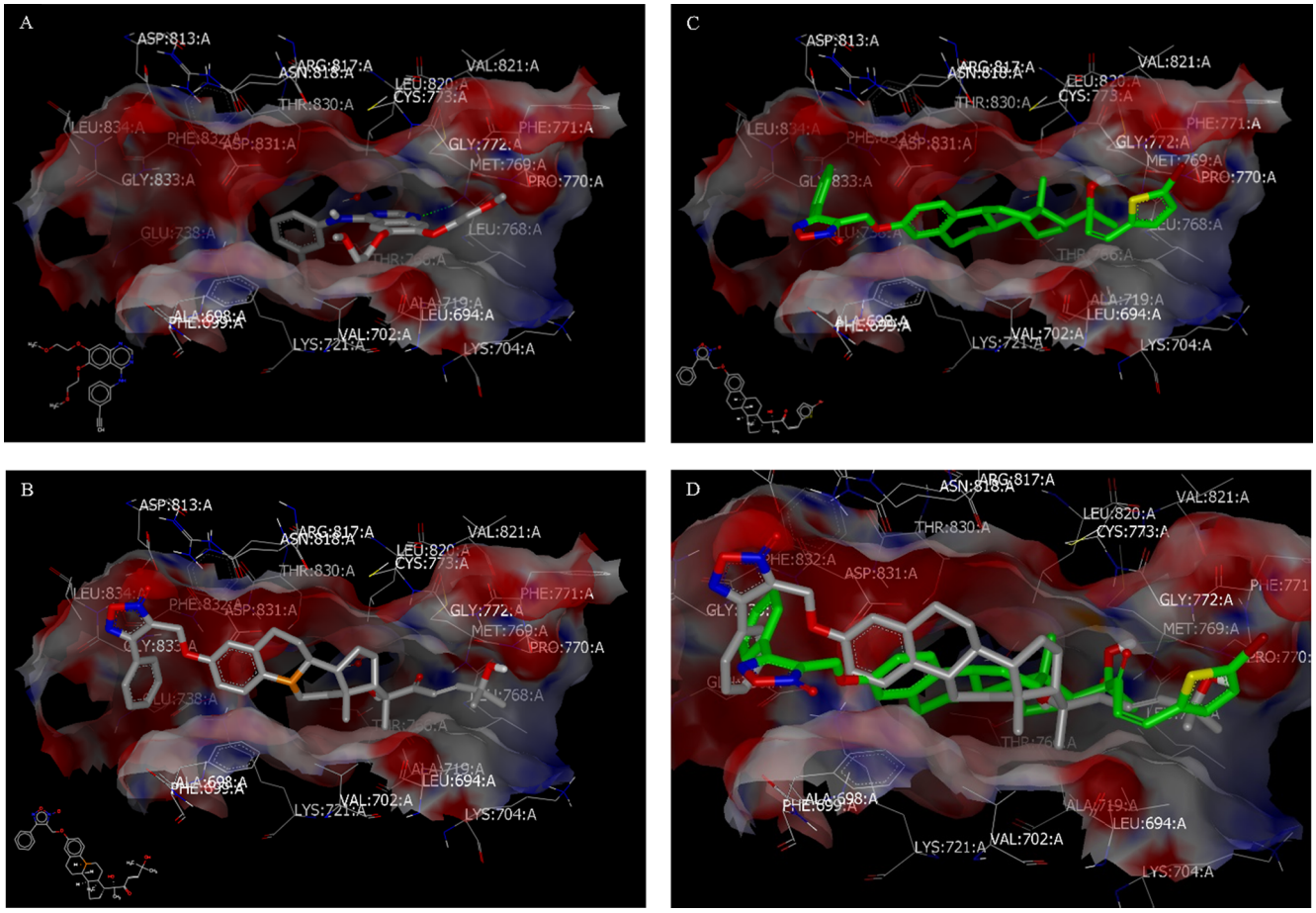

Fig. 3. Visual representation for (A) Erlotinib; (B) NO-CIEA **17**; (C) NO-CIEA **20f** and; (D) overlay of the binding modes of NO-CIEAs **17** (gray) and **20f** (green) docked with PDB: 1M17. These compounds illustrated HB (dashed lines) and hydrophobic-hydrophobic interaction towards EGFR ATP-binding site.

hydroxyl group of commercially available estrone **1** as a *tert*-butyldimethylsilyl (TBS) ether, followed by Wittig reaction with the ketone on ring D to prepare alkene **3** [36]. Hydroxylation of C-19 through hydroboration oxidation with 9-borabicyclo[3.3.1]nonane (9-BBN) upon heating to 60 °C in THF generated the alcohol **4** which was oxidized by PCC into methyl ketone **5** in 92% yield.

Treatment of methyl ketone **5** with catalytic amount of zinc iodide and TMSCN formed the desired nitrile **6** in 90% yield, as diastereomer mixture. The two diastereomers α-hydroxy methyl ketones **7a** (19*R*-isomer) and **7b** (19*S*-isomer) were successfully obtained by nucleophilic addition of methyl lithium to nitrile **6** in dry ether at 0 °C. The diastereomeric mixture was separated by carful column chromatography as they appeared as overlapped spots with ΔR_f less than 0.1 (5% ethyl acetate in hexane). The absolute configuration was determined by NMR and this result is similar to the previous data [26,37]. The 19*R*-isomer is the only isomer that was previously isolated and fully characterized. Herein we report the structural elucidation of 19*S*-isomer by ^{1}H NMR, ^{13}C NMR, ^{13}C DEPT-NMR and HSQC-NMR. The ^{1}H NMR of *S*-isomer showed up-field chemical shift for some signals compared to *R*-one. Among them, the most important hydroxyl proton at C-19 which appeared at 3.49 ppm in case of *S*-isomer while in *R*-isomer it appeared at 3.80 ppm.

In order to install the desired CUCs side chain at C-17, the precursor **11** was synthesized as outlined in Schemes 2. Protection of 2-hyroxy isobutyrate **8** by TBSCl followed by reduction of ester functionality with DIBAL-H to produce primary alcohol **9**. Then, controlled oxidation with either TPAP (Tetrapropylammonium perruthenate) or PCC yielded the protected aldehyde derivative **11**.

On the other hand, to install the NO donor functionality, the furoxan precursor **14** was synthesized as outlined in Scheme 3. Under nitrogen atmosphere, cinnamyl alcohol **12** reacted with sodium nitrite in acetic acid to give 3-(hydroxymethyl)-4-phenyl-1,2,5-oxadiazole 2-oxide **13** which was converted to the corresponding mesylate derivative **14** [38,39].

This set the stage for diverging the syntheses of the estrone analogs by reacting methyl ketone **7a** with an alkyl, aromatic and heterocyclic aldehyde through an aldol condensation to provide the desired α,β-unsaturated ketones. The target compound **17** was synthesized as outlined in Scheme 4 through installing the CUCs side chain at C-17 position then adding the NO donor moiety at the phenolic OH. Optimized reaction conditions in the aldol reaction of ketone **7a** and aliphatic aldehyde **11** required the use of LDA (Lithium diisopropylamide) as a base in THF at −78 °C to produce acyclic α,β-unsaturated ketone **15** in 48% yield. With material in hand, the deprotection of α,β-unsaturated ketone **15** was attempted using tetra-*n*-butylammonium fluoride (TBAF) to afford phenolic derivative **16**. Finally, the furoxan moiety was installed successfully to construct NO-CIEA **17** as depicted in Scheme 4.

Our direction was then oriented to add different aryl aldehydes to examine the effect of aromaticity in CUCs side chain. Aldol condensation of aromatic or heterocyclic aldehydes through enolate formation using sodium hydroxide, Scheme 5, was determined to be optimal here compared to the LDA procedure previously described in Scheme 4. This reaction condition resulted in a greater percent conversion, a higher yield, very short reaction time and a much more economical reagent. Deprotection of acyclic α,β-unsaturated ketones **18a-g** were subjected to a similar TBAF procedure as before to give the phenolic derivatives **19a-g** which reacted finally with furoxan mesylate **14** to give the target

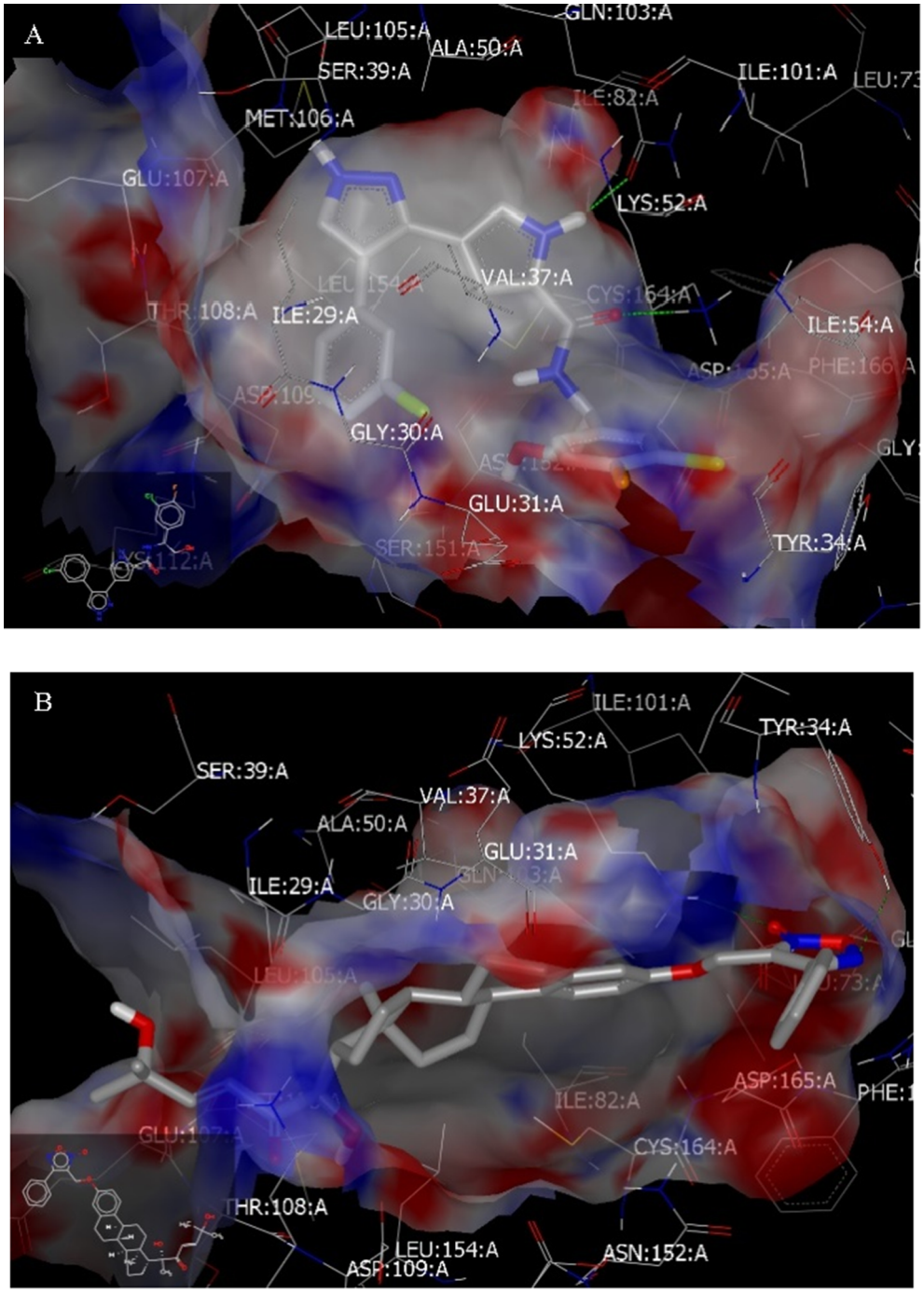

Fig. 4. Visual representation for (A) standard 82A ligand and; (B) NO-CIEA **17** docked with PDB: 2OJJ. The compounds exhibited HB (dashed lines) and hydrophobic-hydrophobic interaction towards glycine-rich loop of ERK.

NO-CIEA **20a-g** in good yields.

To explore the effect of absolute configuration around C-19 on compounds' biological activity, (19*S*)-NO-CIEAs **23a, and 23b** with either strong electron withdrawing group (CF_3) or electron donating group (OCH_3), respectively, were prepared. Aldol condensation of **7b**, with appropriate benzaldehyde derivative, using sodium hydroxide in THF method afforded acyclic α,β-unsaturated ketones **21a,b** which were subjected to TBAF to obtain phenolic derivatives **22a,b**. Finally, coupling them with furoxan mesylate **14** to get the desired (19*S*)-NO-CIEAs **23a,b** in yields 39 and 34%, respectively as depicted in Scheme 6.

For further investigation of SAR, the intermediate **25** was designed and synthesized to study the effect of tethering the estrone base-scaffold with NO donor functionality without CUCs side chain. It was synthesized through deprotection of **7a** with TBAF in THF overnight followed by coupling with furoxan mesylate **14** as outlined in Scheme 7. Moreover, to explore the effect of NO concentration on the anticancer activity, replacement of furoxan moiety with organic dinitrate ester at C-3 position of estrone was designed and synthesized as outlined in Schemes 7. Initially, the phenolic derivative **24** was subjected to O-allylation with allyl bromide to generate the O-allyl derivative **26**. Addition of I_2 (1–3 eq.) to the intermediate **26** at different temperatures failed to synthesize the corresponding diiodo-derivative but in combination with silver nitrate (3 equivalents), the iodonitrate **27** was

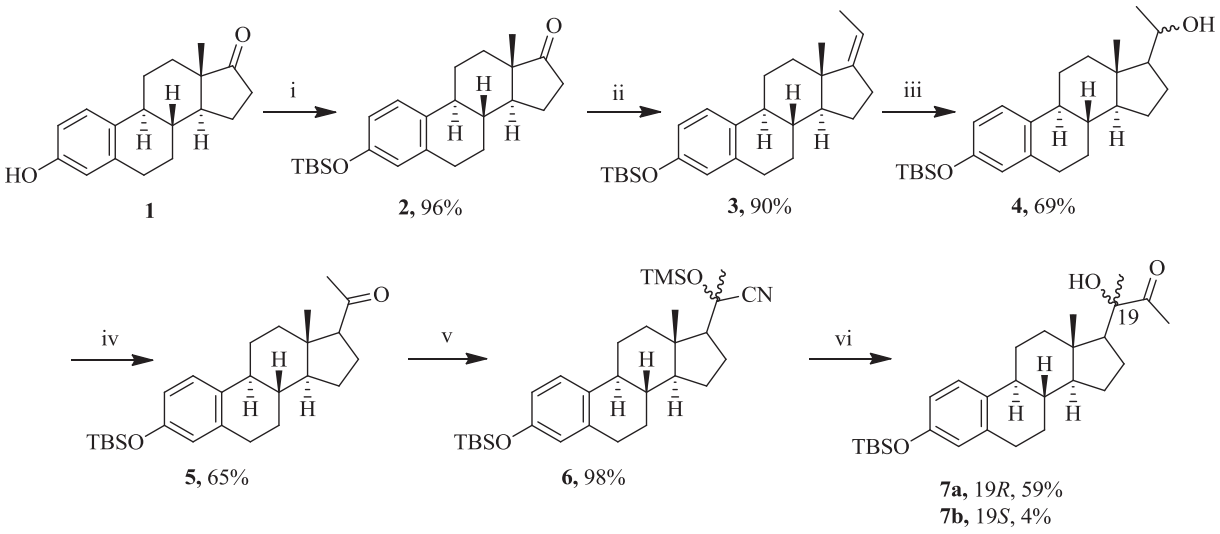

Scheme 1. Synthesis of key intermediates α-hydroxy methyl ketones; (i) TBSCl, imidazole, DMF, overnight, rt; (ii) *t*-BuOK, TEPB, THF, $CH_3CH = PPh_3$, 1 h, reflux (80 °C), 6–7 h; (iii) 9-BBN, THF, 60 °C, 10% NaOH, H_2O_2, rt, 2 h; (iv) PCC, NaOAc, 4 Å MS, DCM, rt; (v) TMSCN, ZnI_2, dry DCM, rt; (vi) MeLi, Et_2O, 0 °C.

successfully synthesized in 86% yield as diastereomeric mixture in the ratio 1:1 (based on quantitative NMR detection). Next, refluxing the intermediate **27** with 3 more equivalents of silver nitrate resulted in 37% of compound **28** as diastereomeric mixture in the ratio of 1:0.5. Finally, the aldol condensation with the selected benzaldehyde derivative (*p*-CF_3PhCHO) in presence of NaOH for 10 min afforded rapidly the target nitrate/CIE hybrid **29**.

Next, our SAR study was extended to prepare the designed analogs **30** and **32** as starting materials for installing the organic dinitrate moiety at C-3 position along with CUCs and *p*-methoxy phenyl side chains at C-17 position, respectively. As shown in Scheme 8, because of the volatility of the aliphatic aldehyde **11**, LDA procedure was used but the reaction proceeded with elimination forming a mixture of compounds **26** and **31**. Their structures were elucidated by ^{1}H NMR, ^{13}C NMR, ^{13}C DEPT-NMR and HSQC-NMR. On the other hand, upon aldol condensation of **27** with *p*-methoxybenzaldehyde using NaOH in dry THF for 10 min, the reaction did not proceed. But after refluxing for 1 h, base-mediated cleavage occurred producing the undesired corresponding phenols **24** and **19d** [40]. Structural elucidations of all separated products were verified by ^{1}H NMR, ^{13}C NMR and ^{13}C DEPT-NMR [37,41].

3.3. Biological evaluation

3.3.1. In vitro antitumor against HepG2 and Erlotinib-resistant HepG2 cell lines

All final NO-CIEAs **17, 20a-g, 23a,b, 25, 28** and **30** were tested for the anticancer activity against both HepG2 (liver cancer cells) and HepG2-R (Erlotinib resistant liver cancer cells) using MTT assay [42–44]. IC_{50} was calculated with regard to DMSO control group and potency was calculated with regard to percentage of antiproliferative activities of Erlotinib and tested compounds, as depicted, in Table 2.

As shown in Table 2, our SAR study showed that some of the tested compounds have high to moderate antitumor activity towards liver cell line (HepG2) with IC_{50} values ranges from 4.69 to 43.28 μM in comparison to Erlotinib as a reference drug (IC_{50} = 25 μM). The NO-CIEA **17** with a hydrophilic cucurbitacin side chain installed at C-17 position of the estrone ring, R configuration around C-19 and tethered with NO releasing furoxan moiety at C-3 position through an ether linkage exhibited the most potent anticancer activity (IC_{50} = 4.69 μM) among the NO-CIEAs as well as the reference drug Erlotinib. The data also revealed that **20a**, (19*R*)-isomer, with strong electron withdrawing *p*-(trifluoromethyl)phenyl group revealed potent anticancer activity with IC_{50} 12.5 μM compared to reference drug Erlotinib (IC_{50} = 25 μM) while its diastereomeric *S*-isomer (compound **23b)** was inactive up to 50 μM.

Moreover, the (19*S*)-isomer **23a** (IC_{50} = 43.82 μM) with electron donating *p*-(methoxy)phenyl group generally exhibited slightly better anticancer activity than the corresponding *R*-one (**20a**; (IC_{50} > 50 μM)), demonstrating that the S configuration analog was a somewhat better substrate for cellular kinases than the R one in this series. Furthermore, introduction of a heterocyclic moiety, like substituted thiophenyl or furyl moieties, did not inhibit the proliferation of HepG2 cells at concentrations as high as 50 μM, indicating that no heterocyclic side chain at the C-17 position favored anticancer activity. Consequently, introducing an aliphatic hydrophilic cucurbitacin side chain at C-17 and tethering the nitric oxide releasing furoxan moiety at C-3 position may have an impact on the binding affinity towards the ATP binding site of EGFR and hydrogen bonding formation and thus increase the ability of the ligands to be more active.

The resistant hepatocellular cancer cells (HepG2-R) was developed in our research group against Erlotinib as standard drug [45]. Hence, all of the final NO-CIEAs were evaluated for their antitumor activity against HepG2-R to study the effect of target compounds on chemotherapeutic resistance using MTT assay. The data revealed that only one analog (**17**) still maintain its cytotoxicity activity against HepG2-R cell line with IC_{50} 8.21 μM compared to sensitive HepG2 cell line (IC_{50} = 4.69 μM).

For further investigation to study SAR of NO-CIEAs, the intermediates **25** and **28** having furoxan and organic dinitrate moieties, respectively, were tested against both HepG2 and HepG2-R cell lines. The data revealed that neither **25** nor **28** inhibited the proliferation at

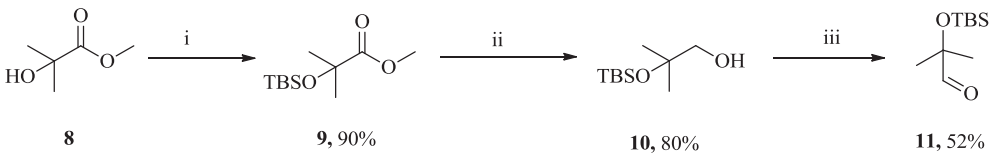

Scheme 2. Synthesis of protected methylpropanal; (i) TBSCl, imidazole, DMF, rt, 3 days; (ii) DIBAL-H, Rochale salt, THF, −78 °C; (iii) condition A: TPAP, NMO, 4 Å MS, 12 h; condition B: PCC, NaOAc, dry DCM, 4 Å, 12 h.

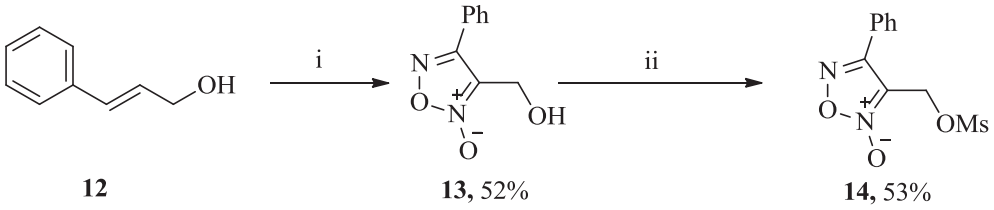

12 **13,** 52% **14,** 53%

Scheme 3. Synthesis of NO-releasing furoxan moiety; (i) $NaNO_2$, HOAc, −10 °C, 24 h; (ii) MsCl, TEA, dry DCM, 0 °C to rt, 2 h.

concentrations as high as 50 μM, indicating that either cucurbitacin or electron with drawing containing aromatic side chain at the C-17 position favored anticancer activity.

Based on variations in compounds' activity related to their diversity in chemical features, the attention was moved to calculate some physiochemical preparties as CLogP and PSA [46,47]. This increasing interest towards lipophilicity can be ascribed to its proven fundamental relevance in absorption, distribution, metabolism, excretion, and toxicity (ADMET) studies. As a consequence, data on lipophilicity is currently being applied in structural information about the biological behavior of drug candidates [48]. As shown in Table 2. NO-CIEA **17** possesses good physicochemical properties (CLogP 6.57 and PSA 118.25) among the target final analogs with a potent broad-spectrum cytotoxicity activity against both HepG2 and HepG2-R cell lines with IC_{50} values 4.69 μM and 8.21 Mμ, respectively. Also, higher, or lower CLogP or PSA values than that of NO-CIEA **17**, showed the lowest cytotoxicity activity.

Our attention was then drawn to examine the coupled precursors of NO-CIEA **17** to determine their potential of cytotoxic activity. Hence, NO releasing furoxan alcohol **13** and compound **16** (des-NO analogs to compound **17**) were examined (Table 3). The data revealed that **13** did not inhibit the proliferation of both cell lines (IC_{50} > 50 μM) while **16** showed IC_{50} 25 and 39.18 μM in HepG2 and HepG2-R cells, respectively, indicating that hybridization favored anticancer activity as well as blocking the estrogenic activity of phenolic derivative through methoxy linkage.

Therefore, tethering NO releasing moiety to cucurbitacin inspired estrone analogs (CIEAs) known of potent *Anti*-proliferation of HCC, will significantly impact the potential anticancer activity of hybrid drug candidate because of synergistic effects of both NO and CIEA. In this context, the designed synthesized novel NO-CIEAs are considered as promising candidates for treatment of HCC and overcoming the chemotherapeutic resistance.

3.3.2. Intracellular measurement of NO release

NO release behavior of compounds **17** and **20a** was examined to indicate whether the strong inhibition of active compounds on the proliferation of tumor cells could be associated with high levels of NO production in HepG2 cells. The latter were exposed to each compound at different concentrations for varying durations (1, 6, 12 and 24 h). The levels of NO produced intracellularly from NO-CIEAs **17** and **20a** along with JS-K (a known NO donor prodrug with two moles NO-releasing diazinium diolate moiety) were examined using NO-sensitive fluorophore, 4-amino-5-(methylamino)-2′,7′-difluorofluorescein diacetate (DAF-FM DA) [43,49–52], (Fig. 5A–C). It was observed that furoxan hybrids **17** and **20a** showed an increase in fluorescence after 1 h of incubation in a dose-dependent manner and produced a significant concentration of NO in tumor cells comparable to JS-K (reference drug). Also, NO-CIEA **17** and **20a** released maximum level of NO at a concentration of 32.92 and 25 μM in comparison to the reference prodrug JS-K which produced the maximum release at 50 μM. Furthermore, the data revealed that there is a significant decrease in NO level at 50 μM after incubation for 1 h with either NO-CIEA **17** or **20a**. In addition, in a dose dependent manner, both NO-CIEAs **17** and **20a** showed a marked decrease in NO level compared to DMSO control after incubation for 6, 12 and 24 h. Obviously, the incubation of cells with the NO-CIEAs **17** and **20a** decreased the overall metabolic activity of the cells, as determined by MTT assay within the concentration range and incubation periods tested; thus, the low NO intracellular content at high concentration of NO donors was caused by their cytotoxicity activity [49]. Moreover, the DAF-FM DA probe was sufficient for detecting the increased fluorescence within a wide range of NO concentrations as was proven by the measurements after 1 h of incubation. This finding document that any potential quenching of the specific DAF-FM DA

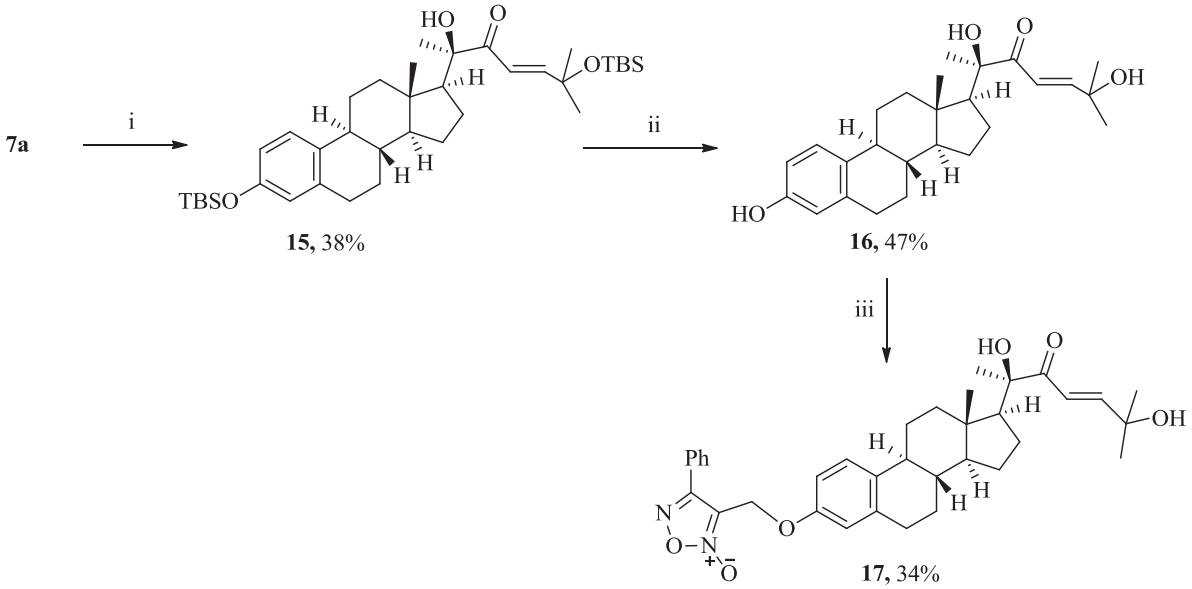

15, 38% **16,** 47% **17,** 34%

Scheme 4. Synthesis of (19*R*)-NO-CIEA **17** with CUCs side chain; (i) LDA, THF, −78 °C, 1 h, **11**, −78 °C to rt, 20 h; (ii) TBAF, THF, rt, 12 h; (iii) NaOH, THF, **14**, reflux, 2 h.

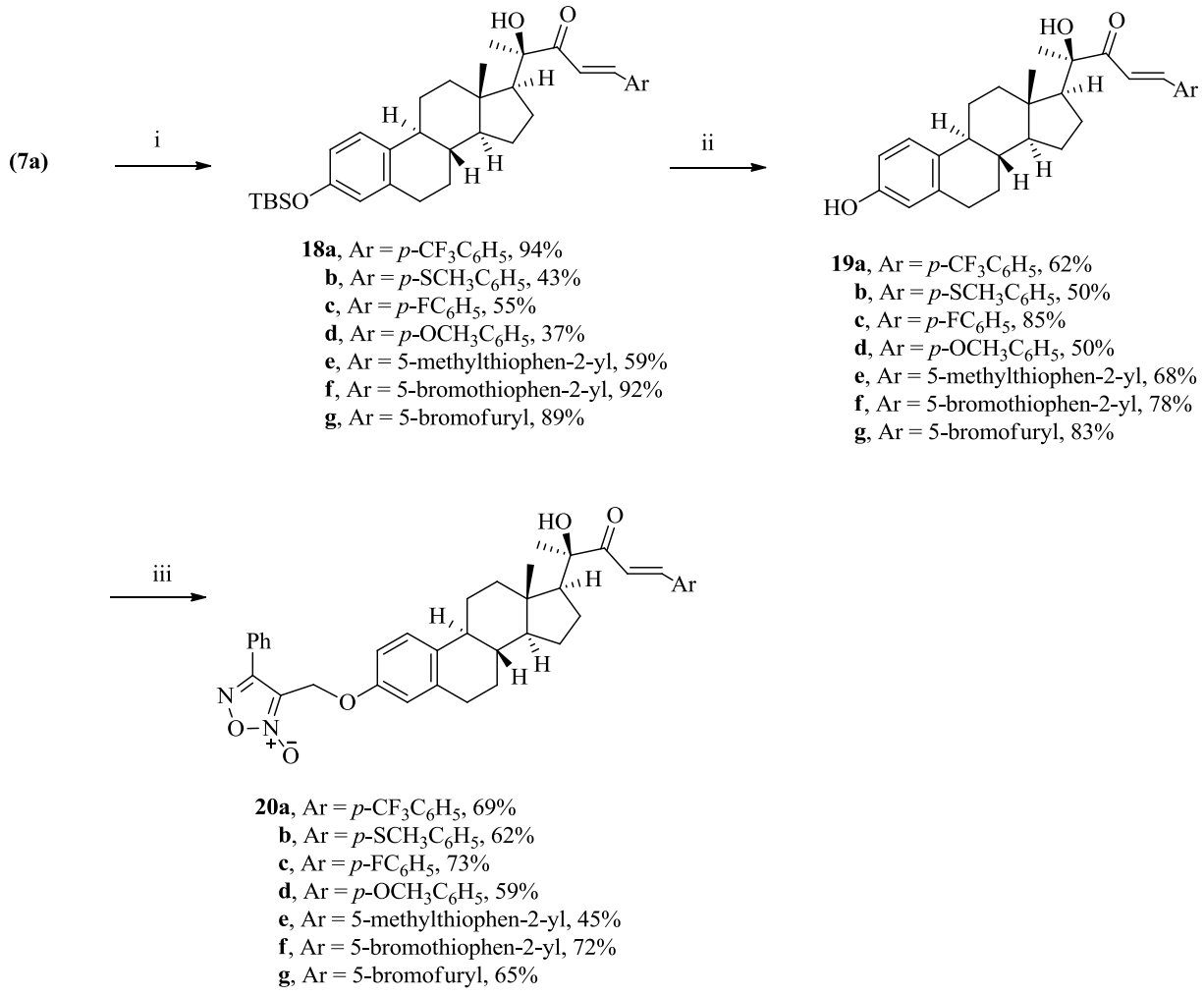

18a, Ar = *p*-$CF_3C_6H_5$, 94%
b, Ar = *p*-$SCH_3C_6H_5$, 43%
c, Ar = *p*-FC_6H_5, 55%
d, Ar = *p*-$OCH_3C_6H_5$, 37%
e, Ar = 5-methylthiophen-2-yl, 59%
f, Ar = 5-bromothiophen-2-yl, 92%
g, Ar = 5-bromofuryl, 89%

19a, Ar = *p*-$CF_3C_6H_5$, 62%
b, Ar = *p*-$SCH_3C_6H_5$, 50%
c, Ar = *p*-FC_6H_5, 85%
d, Ar = *p*-$OCH_3C_6H_5$, 50%
e, Ar = 5-methylthiophen-2-yl, 68%
f, Ar = 5-bromothiophen-2-yl, 78%
g, Ar = 5-bromofuryl, 83%

20a, Ar = *p*-$CF_3C_6H_5$, 69%
b, Ar = *p*-$SCH_3C_6H_5$, 62%
c, Ar = *p*-FC_6H_5, 73%
d, Ar = *p*-$OCH_3C_6H_5$, 59%
e, Ar = 5-methylthiophen-2-yl, 45%
f, Ar = 5-bromothiophen-2-yl, 72%
g, Ar = 5-bromofuryl, 65%

Scheme 5. Synthesis of (19*R*)-NO-CIEAs **20a-g** with aromatic and heterocyclic side chains; (i) ArCHO, NaOH, THF, 105 °C, 10–30 min; (ii) TBAF, THF, rt, 12 h; (iii) **14**, NaOH, THF, reflux, 2 h.

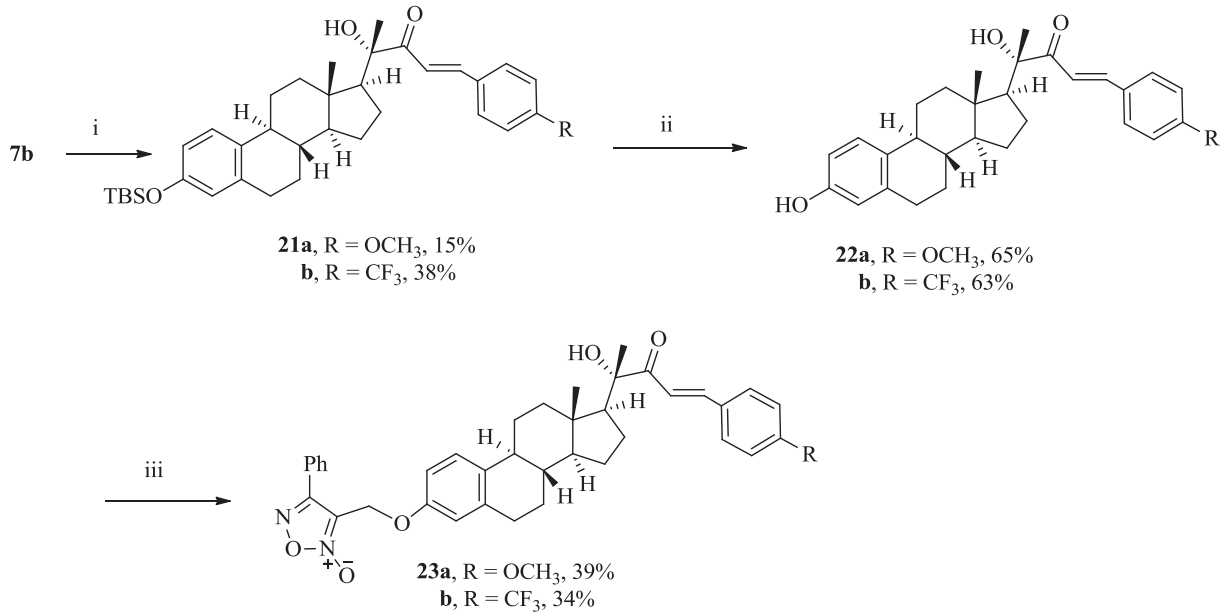

21a, R = OCH_3, 15%
b, R = CF_3, 38%

22a, R = OCH_3, 65%
b, R = CF_3, 63%

23a, R = OCH_3, 39%
b, R = CF_3, 34%

Scheme 6. Synthesis of (19*S*)-NO-CIEAs **23a,b** with aromatic side chain; (i) ArCHO, NaOH, THF, 105 °C, 10–30 min; (ii) TBAF, THF, rt, 12 h; (iii) **14**, NaOH, THF, reflux, 2 h.

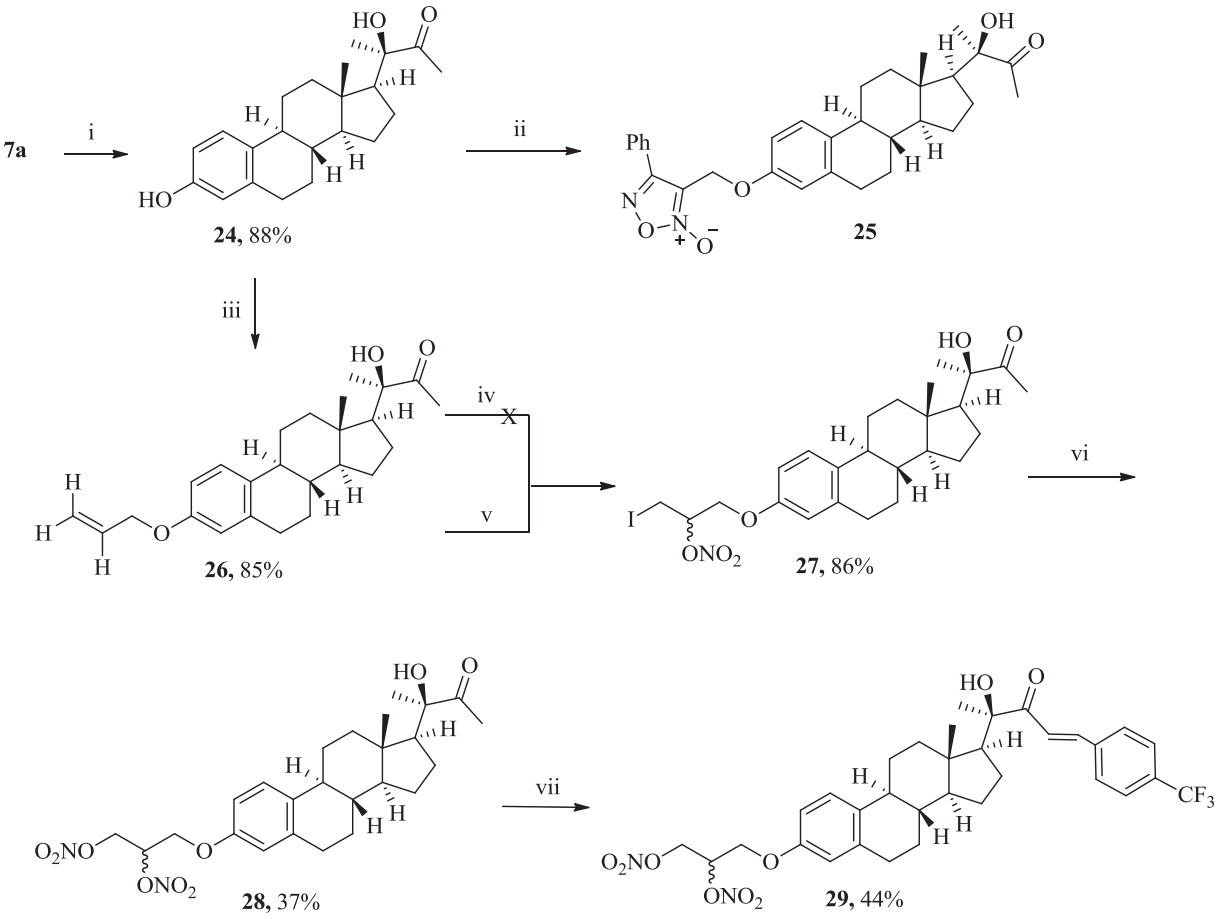

Scheme 7. Synthesis of iodonitrate intermediate **27** and nitrate/CIEA hybrid **29**; (i) TBAF, THF, rt, 12 h; (ii) **14**, NaOH, THF, reflux, 2 h; (iii) allyl bromide, NaOH, THF, reflux, 2 h; (iv) I_2 (1–3 eq.), CH_3CN, rt to reflux, 0.5–1 h; (v) I_2 (1 eq.), CH_3CN (3 eq.), $AgNO_3$ (3 eq.), 30 min, rt; (vi) $AgNO_3$ (3 eq.), CH_3CN, reflux, 7 h; (vii) *p*-CF_3PhCHO, NaOH, THF, 105 °C, 10 min.

fluorescence after incubation for long periods, by increased NO production at higher concentrations of NO-CIEAs **17** and **20a**, did not happen.

Again, we found that among the NO-CIEAs tested, **17** was the most active cytotoxic agent (IC_{50} = 4.69 μM). These results suggest that compound **17** is a far superior source of intracellular NO in comparison with the reference prodrug JS-K.

Additionally, NO-CIEA **17** was tested for its NO releasing activity in HepG2-R cell line and showed the highest level of NO at IC_{50} (8.21 μM) after 1 h of incubation while higher concentrations showed a decrease in fluorescence again (Fig. 5D). Therefore, it is clear to demonstrate that the potent inhibitory effects of NO-CIEA **17** were related to the obvious release of NO in HCC cells line along with cucurbitacin steroidal moiety.

3.3.3. Cell cycle arrest

Flow cytometric analyses of NO-CIEAs **17** and **20a** were conducted to study the effect of these compounds on cell cycle. HepG2 cells were incubated with NO-CIEAs **17** (4.69 μM), **20a** (12.5 μM) and vehicle DMSO (0.01%) as control for 24 h and the cell cycle parameters were conducted. NO-CIEA **17** caused accumulation of cells in G0/G1 phase. As shown in Fig. 6B, NO-CIEA **17** exhibited an increase in the fraction of cells in the G0/G1 phase (63.46% in comparison to 42.06% for the control). Also, it showed a decrease in the proportion of cells in the S phase (26.31% compared to 41.09%) and the G2/M phase (10.22% compared to 16.85%) (Fig. 6A and B). In case of NO-CIEA **20a,** it exhibited also an increase in the fraction of cells in the G0/G1 phase (53.42% compared to 42.06% for the control) and a decrease in the proportion of cells in the S phase (32.00% compared to 41.09%) and the G2/M phase (14.58% compared to 16.85%) (Fig. 6A and C). Briefly, our data showed that both NO-CIEAs **17** and **20a** arrested the cells in G0/G1 phase of cell cycle.

3.3.4. In-cell western analysis (in-cell based ELISA assay)

The effect of the most cytotoxic analog NO-CIEA **17** on EGFR-MAPK signaling pathway was evaluated using In-Cell Western assay (ICW) which is also known as In-Cell Based ELISA Assay (Fig. 7). ICW is an indirect ELISA assay offering a measurement for the levels of two proteins in whole fixed cells without the need for cell lysate. This assay offers a sensitive measurement to be used for adherent and non-adherent cells measuring protein phosphorylation and total protein levels by fluorometric detection method using Odyssey® scanner (LI-COR®) [53–57]. As shown in Fig. 7A–C, the Odyssey images show detection of total proteins regardless of phosphorylation status as well as detection of decreasing amounts of phospho-protein as a function of increasing NO-CIEA **17** concentrations while the graphical representations show the quantification of fluorescence. The data showed the potential activity for NO-CIEA **17** to inhibit the phosphorylation of EGFR, ERK1/2 and MEK1/2 in a dose-dependent manner by about 25%, 29% and 11% inhibition, respectively, compared to untreated cells (Control). Also, the data revealed that there is an initial activation of MEK1/2 phosphorylation at a dose of 1.17 μM and this might be attributed to a partial agonistic activity of NO-CIEA **17** at low doses, Fig. 7C. Thus, NO-CIEA **17** showed a significant dose dependent reduction of EGFR and ERK1/2 phosphorylation in treated cells. This data suggests that the binding ability of the NO-CIEA **17** to the ERK is correlated with the docking

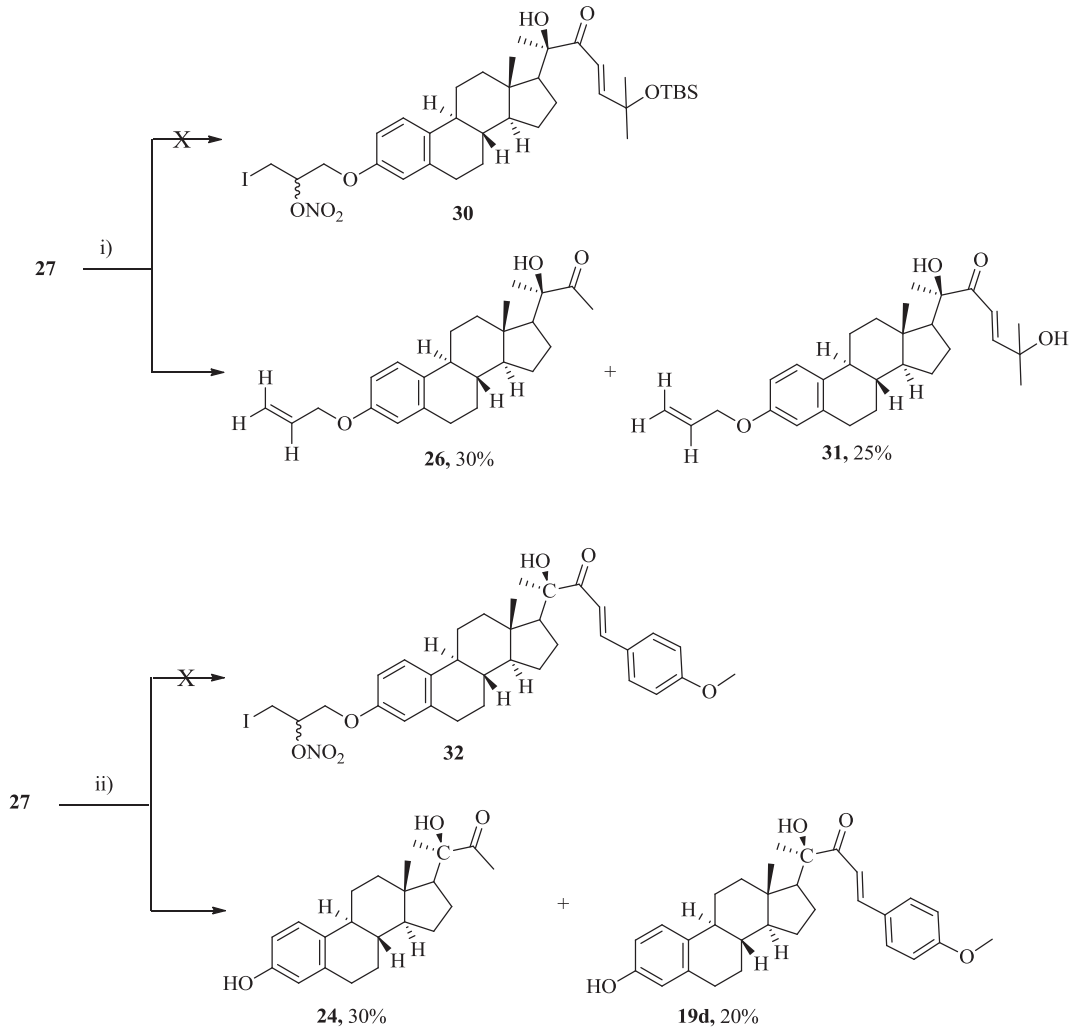

Scheme 8. Unexpected products of aldol condensation with iodonitrate intermediate **27**; (i) LDA, THF, −78 °C, 1 h, **11**, 20 h, rt; (ii) *p*-methoxybenzaldehyde, NaOH, THF, reflux, 1 h.

study and the cell signaling analysis. The higher cytotoxic activity over the cell lines as well as the proper binding towards ERK clearly support our hypothesis that compound **17** is a potential drug candidate for treatment of HCC. Therefore, the NO-CIEA **17** has a potential inhibitory activity towards the MAPK kinase pathway by inhibiting phosphorylated ERK.

3.3.5. Multidrug resistance protein (MRP2) inhibition in HepG2-R cell line

Liver cancer cells have the ability to develop resistance to structurally and mechanistically unrelated drugs over a period of time [58]. MRP2 is the second member of the MRP subfamily of ABC transporter and shares 49% amino acid identity with MRP1 but it has a different expression pattern. Also, MRP2 is highly expressed in the apical (canalicular) hepatocyte plasma membrane [29,59]. Recently, our research group has reported that MRP2 is overexpressed in HepG2-R cell line compared to sensitive one [31] and the expression level of MRP2 was increased in resistant HepG2 cell line to Erlotinib 93% comparing to β-Actin as loading control. It has been reported also by Morrow et al that MRP2 has been expressed in sensitive HepG2 cell line by western blot [60]. Herein, the MRP2 inhibition was evaluated using ICW [53–57]. In a consequence, our attention has been extended to study the effect of NO-CIEA **17** on the chemotherapeutic resistance through exploring its inhibitory effect for MRP2. As shown in Fig. 7D, compound **17** showed a significant reduction of MRP2 expression in a dose dependent manner with 26% inhibition compared to control. Therefore, the NO-CIEA **17** has a significant impact on the chemotherapeutic resistance along with potential inhibitory activity towards the MAPK kinase pathway.

4. Conclusion

In conclusion, a series of NO-CIEAs were designed, synthesized and evaluated for their *anti*-proliferative activity as well as their EGFR-ERK signaling pathway inhibitory activity against hepatocellular carcinoma. Among these compounds, NO-CIEA **17** showed a broad potent spectrum *anti*-proliferative activity against both HepG2 and HepG2-R cell lines (IC_{50} = 4.69 and 8.21 μM, respectively) in comparison to the positive control Erlotinib (IC_{50} = 25 and 47.16 μM, respectively). Also, NO-CIEA **20a** with lipophilic electron-withdrawing group showed remarkably high inhibitory activity against HepG2 cell line (IC_{50} = 12.5 μM) comparable to positive control Erlotinib (IC_{50} = 25 μM) while NO-CIEA **23a** with electron-donating group showed moderate activity (IC_{50} = 43.28 μM). The results indicating that cucurbitacin side chain at C-17 position and NO releasing furoxan moiety linked through alkoxy bridge at C-3 position showed clear SAR. Intracellular measurements of NO using DAF-FM DA revealed that NO-CIEAs **17** and **20a** produced significant amounts of NO after 1 h of incubation in tumor cells comparable to the reference prodrug JS-K. Flow cytometric analysis showed that NO-CIEAs **17** and **20a** mainly arrested the HepG2 cells in the G0/G1 stage. In-Cell Based ELISA screening

Table 2
Anti-proliferative activity of NO-CIEAs **17, 20a-g, 23a,b, 25, 28** and **30** towards HepG2 and HepG2-R cell lines.

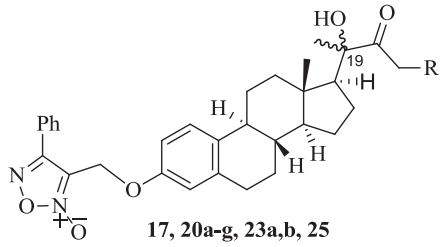

17, 20a-g, 23a,b, 25

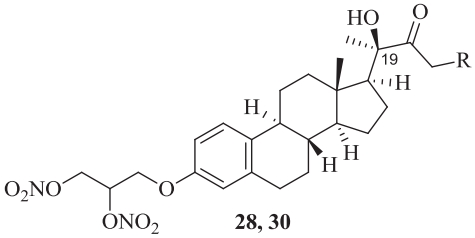

28, 30

Compound No.	C-19	R	IC_{50} (μM)[b]		ClogP[c]	PSA[c,d]
			HepG2	HepG2-R		
17	*R*	(*E*)-2-Hydroxyisobutylidene	4.69 ± 0.48	8.21 ± 0.73	6.57	118.25
20a	*R*	(*E*)-*p*-trifluoromethylbenzylidene	12.50 ± 1.06	> 50	8.75	98.02
20b	*R*	(*E*)-*p*-methylthiobenzylidene	> 50	> 50	8.51	98.02
20c	*R*	(*E*)-*p*-fluorobenzylidene	> 50	> 50	8.33	98.02
20d	*R*	(*E*)-*p*-methoxybenzylidene	> 50	> 50	8.25	107.26
20e	*R*	(*E*)-5-methylthiophen-2-yl-methylidene	> 50	> 50	8.15	98.02
20f	*R*	(*E*)-5-bromothiophen-2-yl-methylidene	> 50	> 50	8.63	98.02
20g	*R*	(*E*)-5-bromofuran-2-yl-methylidene	> 50	> 50	8.21	111.16
23a	*S*	(*E*)-*p*-methoxybenzylidene	43.28 ± 2.98	> 50	8.25	107.26
23b	*S*	(*E*)-*p*-trifluoromethylbenzylidene	> 50	> 50	8.75	98.02
25	*R*	H	> 50	> 50	6.25	98.02
28	*R*	H	> 50	> 50	5.57	156.65
30	*R*	(*E*)-*p*-trifluoromethylbenzylidene	> 50	> 50	8.37	156.65
Erlotinib[a]	–	–	25.00 ± 0.47	47.16 ± 3.02	2.79	74.75
CUCs D	–	–	26.00 ± 0.20	–	2.13	132.12
JS-K	–	–	7.00 ± 0.01[52]	17.84 ± 1.58	1.99	174.78

[a] Positive control.
[b] IC_{50}: concentration of the test compound that inhibits 50% of cell growth (results are expressed as the mean ± SD (n = 3).
[c] Calculated by Molinspiration.
[d] Molecular polar surface area.

Table 3
Anti-proliferative activity of compound **13** and des-NO-CIEA **16** towards HepG2 and HepG2-R cell lines.

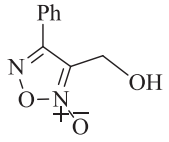

13

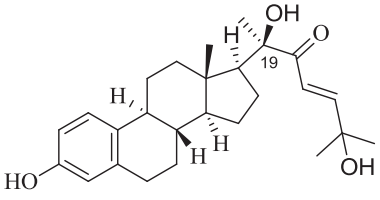

16

Compound No.	IC_{50} (μM)[b]		ClogP[c]	PSA[c,d]
	HepG2	HepG2-R		
13	> 50	> 50	1.60	71.72
16	24.87 ± 2.35	39.18 ± 2.57	4.11	77.75
Erlotinib[a]	25.00 ± 0.47	47.163 ± 3.02	2.79	74.75

[a] Positive control.
[b] IC_{50}: concentration of the test compound that inhibits 50% of cell growth (results are expressed as the mean ± SD (n = 3).
[c] Calculated by Molinspiration [74].
[d] Molecular polar surface area.

showed that NO-CIEA **17** has a potential inhibitory activity towards both EGFR and MAPK pathway by inhibiting both phosphorylated EGFR and ERK, respectively. This data suggests the binding ability of the NO-CIEA **17** to both EGFR and ERK to be well correlated along with the docking study and the cell signaling analysis. Also, it showed a significant reduction of MRP2 expression by about 26% in comparison to control. Therefore, the NO-CIEA **17** has a significant impact on the chemotherapeutic resistance along with potential inhibitory activity towards the EGFR-MAPK pathway.

5. Experimental procedures

5.1. Chemistry

^{1}H and ^{13}C NMR spectra were acquired on a Bruker AVANCE-400 or 600 MHz NMR spectrometer, in DMSO-d_6, $CDCl_3$ or $(CD_3)_2CO$ using the solvent residual peak as the internal standard, with the reporting of coupling constants in Hz and the signal multiplicities are reported as singlet (s), doublet (d), triplet (t), quartet (q), doublet of doublets (dd), doublet of triplets (dt), multiplet (m), or broad (br). HRMS data was obtained using EI ionization on a ThermoFinnigan MAT 95 XL mass spectrometer. TLC analysis was performed using pre-coated silica gel PE sheets. Products were purified via column chromatography using silica gel 40–63 μm (230–400 mesh) and prep-plates (Alltech preparative column, Econosil C18 10u, length 250 mm, ID 22 mm). All reagents and solvents were obtained from commercial suppliers and used as received. All chemical reactions requiring anhydrous conditions were performed with oven-dried glassware under an atmosphere of nitrogen.

Compounds **2–6** [37], **7a** [37], **9–11** [61], **13** [38], **15** [37], **16** [37], **18a,c,d, 19a,c,d, 21a-c, 22a-c** and **24** [37,41] and **27** [37] were prepared as reported by our research group.

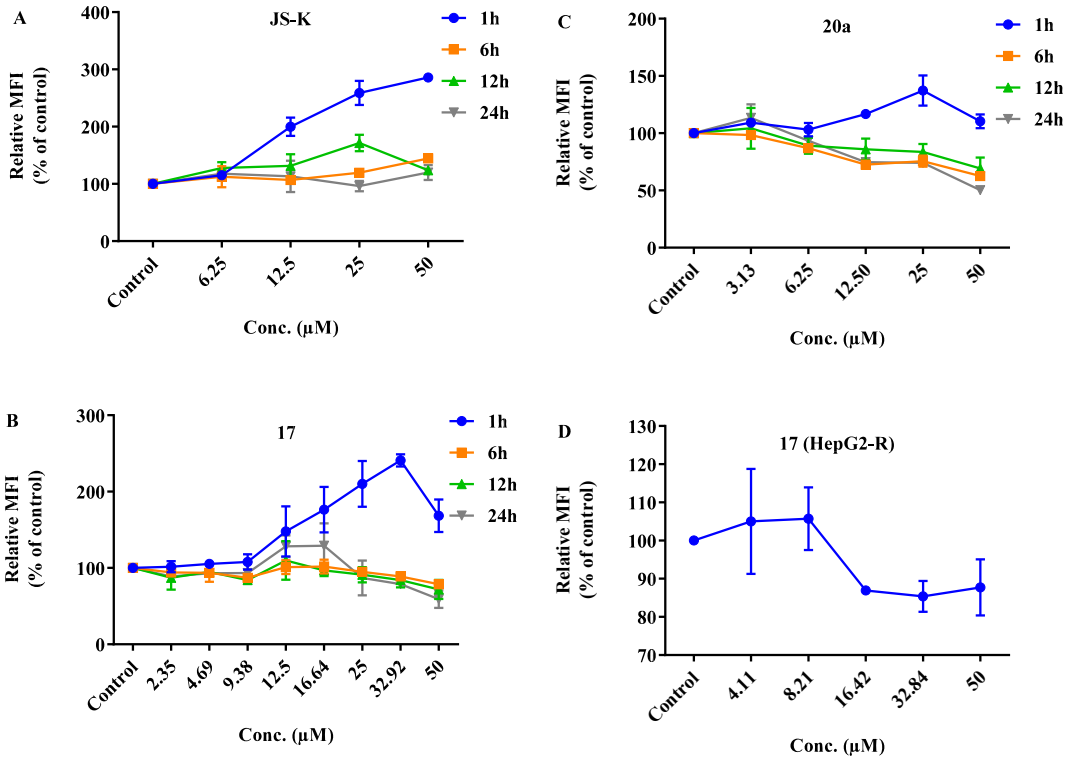

Fig. 5. Intracellular NO release in HepG2 and HepG2-R cells as measured by DAF-FM DA assay. (a) JS-K (reference drug); (b) NO-CIEA **17** against HepG2 cells and; (c) NO-CIEA **20a** against HepG2 cells. (d) NO-CIEA **17** against HepG2-R cells. Values reported are averages ± SD of at least two measurements.

*5.1.1. General procedure for preparation of the key intermediates (R/S) α-hydroxy methyl ketones (**7b**)*

To a stirred solution of cyanohydrin **6** (6.9468 g, 6.95 mmol) in a dry ether (20 mL), methyl lithium (MeLi) (1.6 M in ether, 13.03 mL, 20.85 mmol) was added dropwise at 0 °C. The reaction mixture was allowed to stir for 2 h at 0 °C, then quenched by adding glacial acetic acid (2.6 mL) in one portion at 0 °C and allowed to stir for 30 min at 0 °C. Saturated sodium bicarbonate solution was added to neutralize the acidic mixture. Ethyl acetate was used to extract the aqueous layer (3x50 mL), dried under sodium sulfate anhydrous, then concentrated under *vacuo* [37]. The resulted diastereomers were purified by silica gel column chromatography (5% ethyl acetate in hexane) to give the key intermediates α-hydroxyl ketone **7a** (19*R*-isomer; 59%) and **7b** (19*S*-isomer; 4%).

7b; colorless crystals; yield 4%; ^{1}H NMR (600 MHz, $CDCl_3$) δ 6.89 (d, J = 8.4 Hz, 1H), 6.42 (dd, J = 8.4, 2.6 Hz, 1H), 6.36 (d, J = 2.6 Hz, 1H), 3.49 (s, 1H), 2.66–2.56 (m, 2H), 2.14 (s, 3H), 2.02–1.86 (m, 3H), 1.76–1.65 (m, 3H), 1.60–1.55 (m, 1H), 1.49 (dt, J = 11.9, 3.2 Hz, 1H), 1.26–1.18 (m, 2H), 1.15 (s, 3H), 1.09–0.98 (m, 3H), 0.79 (s, 9H), 0.55 (s, 3H), 0.00 (s, 6H). ^{13}C NMR (151 MHz, $CDCl_3$) δ 212.88, 153.33, 137.81, 132.95, 125.98, 119.97, 117.13, 79.82, 56.41, 55.61, 43.73, 42.80, 38.73, 37.91, 29.63, 27.65, 26.41, 26.16, 25.73, 25.11, 22.86, 22.60, 18.19, 12.90, −4.37. ^{13}C DEPT-NMR (151 MHz, $CDCl_3$) δ 125.98, 119.97, 117.13, 56.41, 55.61, 43.73, 38.72 (inverted CH_2), 37.91, 29.63 (inverted CH_2), 27.65 (inverted CH_2), 26.42, 26.16 (inverted CH_2), 25.73, 25.11, 22.86 (inverted CH_2), 22.60 (inverted CH_2), 12.90, −4.37.

*5.1.2. General procedure for preparation of 3-(((methylsulfonyl)oxy) methyl)-4-phenyl-1,2,5-oxadiazole 2-oxide (**14**)*

Triethylamine (0.62 mL, 4.43 mmol) was added to furoxan alcohol (284 mg, 1.48 mmol) in dry CH_2Cl_2 (10 mL) at 0 °C followed by

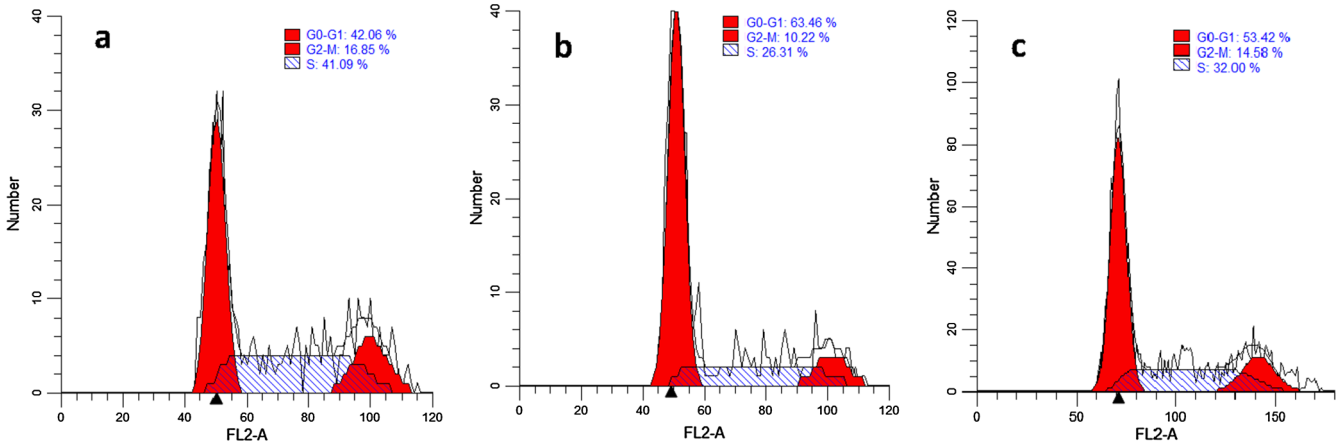

Fig. 6. Flow cytometric analysis of cell cycle parameters of HepG2 cells incubated for 24 h; (a) control; (b) 4.69 µM (IC_{50}) of NO-CIEA **17**; (c) 12.5 µM (IC_{50}) of NO-CIEA **20a**.

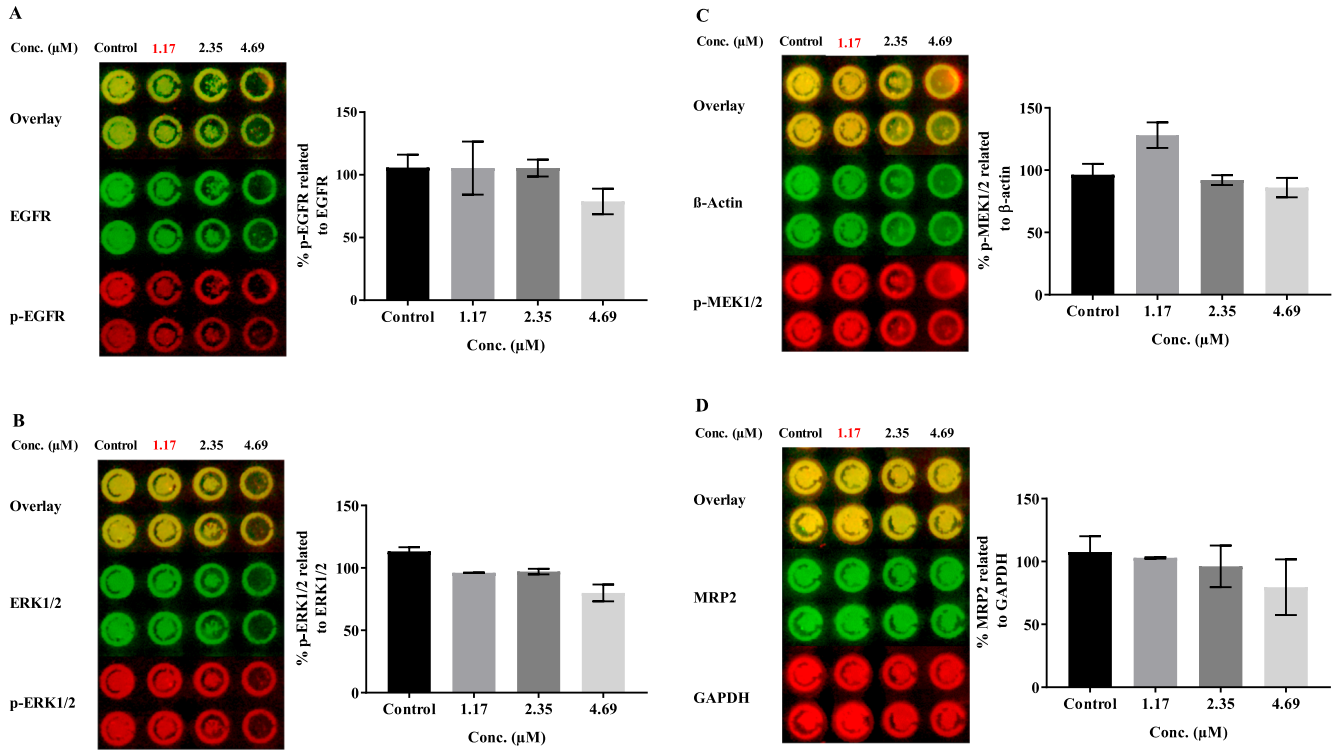

Fig. 7. In-Cell Western analysis of predicted protein targets of NO-CIEA **17**. (A) Analysis of EGFR phosphorylation in HepG2 cells; ICW plate image and p-EGFR intensity in 800 channel was normalized to total EGFR intensity in 700 channel. (B) Analysis of ERK1/2 phosphorylation in HepG2 cells; ICW plate image and p-ERK1/2 intensity in 800 channel was normalized to total ERK1/2 intensity in 700 channel. (C) Analysis of MEK1/2 phosphorylation in HepG2 cells; ICW plate image and p-MEK1/2 intensity in 700 channel was normalized to β-actin intensity in 800 channel. (D) Analysis of MRP2 inhibition in HepG2-R cells; ICW plate image and MRP2 intensity in 800 channel was normalized to GAPDH intensity in 700 channel. Values reported are averages ± SD of at least two measurements.

dropwise addition of MsCl (0.17 mL, 2.2 mmol) over 10 min. The mixture was allowed to warm to room temperature and stirred for 3 h. The reaction was quenched with saturated aqueous NH_4OH (10 mL) and extracted with ethyl acetate (3 × 75 mL). Combined organic layers washed with brine (2 × 15 mL), dried over anhydrous Na_2SO_4, and concentrated under *vacuo* to give yellow oil [38]. The desired product was isolated by column chromatography (hexane/ethyl acetate; 9.5:0.5) as yellow oil which solidifies upon freezing yielding furoxan mesylate **14** as yellow crystals (53%). ^{1}H NMR (400 MHz, $CDCl_3$) δ 7.67 (m, 5H), 4.57 (s, 2H). ^{13}C NMR (101 MHz, $CDCl_3$) δ 156.06, 131.66, 129.60, 127.56, 125.63, 113.07, 32.84.

*5.1.3. General procedure for preparation of (R,E)-4-((8S,9S,13S,14S,17S)-3-((tert-butyldimethylsilyl)oxy)-13,17-dimethyl-7,8,9,11,12,13,14,15,16,17-decahydro-6H-cyclopenta[a]phenanthren-17-yl)-4-hydroxy-1-(aryl)pent-1-en-3-one **(18b, 24a,b)***

To a solution of α-hydroxy methyl ketone **7a,b** (0.1836 g, 0.4 mmol) in THF (1 mL) in an open 20 mL-glass vial, substituted aromatic/heterocyclic aldehyde (0.8 mmol) and sodium hydroxide (0.0464 g, 1.16 mmol) were added at room temperature and the reaction mixture was then heated at 105 °C for 20–30 min with continuing addition of THF by an approximate rate of 0.5 mL/min (avoid dryness; TLC monitoring). The reaction mixture was then quenched by the addition of water (15 mL), followed by extraction with EtOAc (3 × 20 mL), washed with brine, dried with anhydrous Na_2SO_4, and concentrated in *vacuo* [37,62–64]. The crude product was purified by silica gel column chromatography with hexanes/EtOAc (9.5:0.5) to yield the corresponding TBS protected enones **18b** and **24a,b**.

*5.1.3.1. (R,E)-4-((8S,9S,13S,14S,17S)-3-((tert-butyldimethylsilyl)oxy)-13,17-dimethyl-7,8,9,11,12,13,14,15,16,17-decahydro-6H-cyclopenta[a]phenanthren-17-yl)-4-hydroxy-1-(4-(methylthio)phenyl)pent-1-en-3-one **(18b)***. White solid; 43% yield; ^{1}H NMR (600 MHz, $CDCl_3$) δ 7.61 (d, J = 15.5 Hz, 1H), 7.33 (d, J = 8.4 Hz, 2H), 7.05 (d, J = 8.4 Hz, 2H), 6.94 (d, J = 8.4 Hz, 1H), 6.81 (d, J = 15.5 Hz, 1H), 6.43 (dd, J = 8.4, 2.5 Hz, 1H), 6.36 (d, J = 2.5 Hz, 1H), 4.03 (s, 1H), 2.66–2.56 (m, 2H), 2.31 (s, 3H), 2.16–1.99 (m, 3H), 1.71–1.62 (m, 2H), 1.47–1.38 (m, 3H), 1.36 (s, 3H), 1.35–1.32 (m, 1H), 1.15–1.03 (m, 5H), 0.79 (s, 9H), 0.78 (s, 3H), −0.00 (s, 6H). ^{13}C NMR (151 MHz, $CDCl_3$) δ 201.87, 153.34, 145.18, 143.12, 137.87, 133.17, 130.74, 129.05, 126.05, 125.91, 120.01, 117.31, 117.17, 79.15, 55.79, 55.17, 44.36, 43.92, 40.76, 38.11, 29.66, 27.68, 26.64, 25.78, 24.43, 23.70, 22.08, 18.23, 15.10, 13.70, −4.32.

*5.1.3.2. (S,E)-4-((8S,9S,13S,14S,17S)-3-((tert-butyldimethylsilyl)oxy)-13-methyl-7,8,9,11,12,13,14,15,16,17-decahydro-6H-cyclopenta[a]phenanthren-17-yl)-4-hydroxy-1-(4-methoxyphenyl)pent-1-en-3-one **(21a)***. White solid; 15% yield; ^{1}H NMR (400 MHz, $CDCl_3$) δ 7.67 (d, J = 15.6 Hz, 1H), 7.43 (d, J = 8.7 Hz, 2H), 6.86–6.75 (m, 4H), 6.42–6.33 (m, 2H), 3.81 (s, 1H), 3.68 (s, 3H), 2.65–2.62 (m, 2H), 2.05–1.74 (m, 3H), 1.73–1.55 (m, 2H), 1.52–1.33 (m, 3H), 1.22 (s, 3H), 1.19–1.02 (m, 6H), 0.80 (s, 9H), 0.61 (s, 3H), 0.04–0.00 (m, 6H). ^{13}C NMR (101 MHz, $CDCl_3$) δ 202.78, 162.01, 153.26, 144.14, 137.79, 133.10, 130.47, 127.18, 126.03, 119.92, 117.76, 117.10, 114.54, 79.07, 56.38, 55.67, 55.47, 43.76, 43.06, 39.25, 37.95, 29.69, 27.70, 26.54, 25.74, 22.93, 22.69, 18.18, 14.18, 13.37, −4.37.

*5.1.3.3. (S,E)-4-((8S,9S,13S,14S,17S)-3-((tert-butyldimethylsilyl)oxy)-13-methyl-7,8,9,11,12,13,14,15,16,17-decahydro-6H-cyclopenta[a]phenanthren-17-yl)-4-hydroxy-1-(4-(trifluoromethyl)phenyl)pent-1-en-3-one **(24b)***. White solid; 38% yield; ^{1}H NMR (600 MHz, $CDCl_3$) δ 7.43 (d, J = 8.2 Hz, 2H), 7.33 (d, J = 8.2 Hz, 2H), 6.86 (d, J = 8.5 Hz, 1H), 6.68 (d, J = 15.8 Hz, 1H), 6.41 (dd, J = 8.5, 2.5 Hz, 1H), 6.37 (d, J = 2.5 Hz, 1H), 6.23 (d, J = 15.8 Hz, 1H), 4.25 (s, 1H), 2.69–2.59 (m,

2H), 2.10–1.93 (m, 2H), 1.85–1.80 (m, 2H), 1.73–1.68 (m, 2H), 1.54–1.50 (m, 1H), 1.36 (s, 3H), 1.34–1.28 (m, 2H), 1.24–1.09 (m, 5H), 0.79 (s, 9H), 0.66 (s, 3H), −0.00 (s, 6H). ^{13}C NMR (151 MHz, $CDCl_3$) δ 213.04, 153.42, 139.74, 137.62, 132.56, 131.70, 129.82, 126.76, 126.07, 125.73, 125.71, 119.98, 117.22, 79.70, 56.23, 55.91, 47.42, 43.58, 39.76, 38.59, 29.58, 28.96, 27.91, 26.53, 25.73, 25.10, 24.87, 18.20, 13.82, −4.37.

*5.1.4. General procedure for preparing of (R,E)-4-hydroxy-4-((8S,9S,13S,14S,17S)-3-hydroxy-13-methyl-7,8,9,11,12,13,14,15,16,17-decahydro-6H-cyclopenta[a]phenanthren-17-yl)-1-(aryl or Het.)pent-1-en-3-one **(19b** and **22a,b)***

To a stirred solution of protected enones **7a**, **16** and **21a,b** (0.18 mmol) in THF (5 mL), TBAF (0.53 mL, 0.53 mmol, 1 M in THF) was added and stirred for 12 h. The reaction mixture was then quenched with saturated ammonium chloride solution and extracted with ethyl acetate (3x20 mL), washed with brine, dried over anhydrous sodium sulfate, filtrated, and concentrated under *vacuo* [37]. Silica gel column chromatography was used to purify the crude material (hexanes/EtOAc; 8:2) to provide the corresponding phenolic enones **19b** and **22a,b**.

*5.1.4.1. (R,E)-4-hydroxy-4-((8S,9S,13S,14S,17S)-3-hydroxy-13-methyl-7,8,9,11,12,13,14,15,16,17-decahydro-6H-cyclopenta[a]phenanthren-17-yl)-1-(4-(methylthio)phenyl)pent-1-en-3-one **(19b)***. White solid; 50% yield; ^{1}H NMR (600 MHz, $CDCl_3$) δ 7.72 (d, J = 15.6 Hz, 1H), 7.44 (d, J = 8.5 Hz, 2H), 7.16 (d, J = 8.5 Hz, 2H), 7.07 (d, J = 8.4 Hz, 1H), 6.92 (d, J = 15.6 Hz, 1H), 6.56 (dd, J = 8.4, 2.7 Hz, 1H), 6.48 (d, J = 2.7 Hz, 1H), 5.16 (s, 1H), 4.22 (s, 1H), 2.77–2.67 (m, 2H), 2.43 (s, 3H), 2.27–2.09 (m, 3H), 1.82–1.73 (m, 2H), 1.57–1.50 (m, 3H), 1.49 (s, 3H, C20-*H*$_3$), 1.35–1.32 (m, 1H), 1.24–1.15 (m, 5H), 0.89 (s, 3H). ^{13}C NMR (151 MHz, $CDCl_3$) δ 201.95, 153.47, 145.40, 143.19, 138.26, 132.64, 130.67, 129.08, 126.44, 125.89, 117.19, 115.32, 112.70, 79.27, 55.71, 55.17, 44.33, 43.84, 40.69, 38.13, 29.64, 27.58, 26.67, 24.34, 23.65, 22.05, 15.09, 13.67.

*5.1.4.2. (S,E)-4-hydroxy-4-((8S,9S,13S,14S,17S)-3-hydroxy-13-methyl-7,8,9,11,12,13,14,15,16,17-decahydro-6H-cyclopenta[a]phenanthren-17-yl)-1-(4-methoxyphenyl)pent-1-en-3-one **(22a)***. White solid; 65% yield; ^{1}H NMR (400 MHz, Acetone) δ 7.75 (s, 1H), 7.60–7.56 (m, 3H, Ar-*H*), 7.19 (d, J = 15.7 Hz, 1H), 6.82 (d, J = 8.9 Hz, 2H), 6.79 (d, J = 8.4 Hz, 1H), 6.35 (dd, J = 8.4, 2.6 Hz, 1H), 6.31 (d, J = 2.6 Hz, 1H), 3.82 (s, 1H), 3.67 (s, 3H), 2.64–2.47 (m, 2H), 2.02–1.89 (m, 3H), 1.78–1.61 (m, 2H), 1.60–1.26 (m, 3H), 1.16 (s, 3H), 1.13–0.96 (m, 6H), 0.58 (s, 1H). ^{13}C NMR (101 MHz, Acetone) δ 162.93, 155.92, 144.05, 138.33, 131.99, 131.51, 128.38, 126.99, 119.52, 115.92, 115.33, 113.55, 79.82, 56.64, 56.28, 55.86, 44.60, 43.68, 39.96, 39.17, 28.52, 27.17, 26.98, 23.63, 23.16, 13.95.

*5.1.4.3. (S,E)-4-hydroxy-4-((8S,9S,13S,14S,17S)-3-hydroxy-13-methyl-7,8,9,11,12,13,14,15,16,17-decahydro-6H-cyclopenta[a]phenanthren-17-yl)-1-(4-(trifluoromethyl)phenyl)pent-1-en-3-one **(22b)***. White solid; 63% yield; ^{1}H NMR (600 MHz, $CDCl_3$) δ 7.53 (d, J = 8.2 Hz, 2H), 7.42 (d, J = 8.2 Hz, 2H), 6.98 (d, J = 8.4 Hz, 1H), 6.77 (d, J = 15.9 Hz, 1H), 6.51 (dd, J = 8.4, 2.6 Hz, 1H), 6.47 (d, J = 2.6 Hz, 1H), 6.32 (d, J = 15.9 Hz, 1H), 4.83 (s, 1H), 4.40 (s, 1H), 2.80–2.66 (m, 2H), 2.09–1.90 (m, 3H), 1.83–1.78 (m, 2H), 1.63–1.61 (m, 1H), 1.46 (s, 3H), 1.43–1.10 (m, 8H), 0.76 (s, 3H). ^{13}C NMR (151 MHz, $CDCl_3$) δ 213.05, 153.45, 138.05, 132.15, 131.58, 129.92, 126.86, 126.77, 126.47, 125.73, 125.71, 115.27, 112.72, 79.75, 56.21, 55.83, 47.40, 43.49, 39.70, 38.62, 29.56, 28.96, 27.80, 26.60, 25.03, 24.85, 13.79.

*5.1.5. General procedure for preparing of 3-((((8S,9S,13S,14S,17S)-17-((R,E)-5-(aryl or Het.)-2-hydroxy-3-oxopent-4-en-2-yl)-13-methyl-7,8,9,11,12,13,14,15,16,17-decahydro-6H-cyclopenta[a]phenanthren-3-yl)oxy)methyl)-4-phenyl-1,2,5-oxadiazole 2-oxide **(17, 20a-g, 23a,b** and **25)***

To a stirred solution of phenolic enones **16, 19a-g, 22a,b** and **24** (0.28 mmol) in THF (10 mL), sodium hydroxide (0.011 g, 0.28 mmol) and furoxan mesylate **14** (0.150 g, 0.56 mmol) were added. The reaction mixture was heated under reflux for 1 h. then another 0.011 g (0.28 mmol) of sodium hydroxide was added and the reflux was continued for another 1 h (TLC monitoring). The reaction mixture was quenched with water and extracted with ethyl acetate (3x20 mL), washed with brine, dried over sodium sulfate anhydrous, filtrated, and concentrated under *vacuo* [38,65–67]. Silica gel column chromatography was used to purify the crude materials to afford the corresponding titled NO-CIEAs (30% ethyl acetate in hexane for **17** and 15% ethyl acetate in hexane for **20a-g, 23a,b** and **25**).

*5.1.5.1. 3-((((8S,9S,13S,14S)-17-((R,E)-2,6-dihydroxy-6-methyl-3-oxohept-4-en-2-yl)-13-methyl-7,8,9,11,12,13,14,15,16,17-decahydro-6H-cyclopenta[a]phenanthren-3-yl)oxy)methyl)-4-phenyl-1,2,5-oxadiazole 2-oxide **(17)***. Yellowish white solid; 34% yield; ^{1}H NMR (600 MHz, $CDCl_3$) δ 7.79 (dd, J = 8.2, 1.4 Hz, 2H), 7.49–7.42 (m, 3H), 7.15 (d, J = 8.5 Hz, 1H), 7.08 (d, J = 15.2 Hz, 1H), 6.71 (dd, J = 8.5, 2.8 Hz, 1H), 6.64 (d, J = 2.8 Hz, 1H), 6.62 (d, J = 15.2 Hz, 1H), 4.99 (s, 2H), 4.05 (s, 1H), 2.82–2.72 (m, 2H), 2.27–2.19 (m, 2H), 2.16–2.10 (m, 1H), 1.97 (s, 1H), 1.81–1.74 (m, 2H), 1.62–1.56 (m, 2H), 1.52–1.48 (m, 3H), 1.42 (s, 3H), 1.33 (s, 6H), 1.18 (m, 3H), 0.87 (s, 3H), 0.80 (dd, J = 7.0, 3.2 Hz, 3H). ^{13}C NMR (151 MHz, $CDCl_3$) δ 202.34, 157.16, 156.02, 154.84, 138.55, 134.60, 131.36, 129.35, 127.78, 126.65, 126.26, 118.10, 114.93, 112.28, 112.25, 79.19, 71.36, 58.32, 55.63, 54.62, 44.28, 43.83, 40.55, 37.99, 29.76, 29.56, 29.51, 27.49, 26.59, 24.17, 23.67, 21.98, 13.63. HRESI-MS m/z calcd for $[M+Na]^+$ $C_{35}H_{42}N_2O_6$: 609.293508, found: 609.295609.

*5.1.5.2. 3-((((8S,9S,13S,14S,17S)-17-((R,E)-2-hydroxy-3-oxo-5-(4-(trifluoromethyl)phenyl)pent-4-en-2-yl)-13-methyl-7,8,9,11,12,13,14,15,16,17-decahydro-6H-cyclopenta[a]phenanthren-3-yl)oxy)methyl)-4-phenyl-1,2,5-oxadiazole 2-oxide **(20a)***. Yellow solid; 69% yield; ^{1}H NMR (600 MHz, $CDCl_3$) δ 7.81–7.79 (m, 2H), 7.77 (d, J = 15.7 Hz, 1H), 7.65 (d, J = 8.4 Hz, 2H), 7.61 (d, J = 8.4 Hz, 2H), 7.47 (m, 3H), 7.17 (d, J = 8.6 Hz, 1H), 7.04 (d, J = 15.7 Hz, 1H), 6.73 (dd, J = 8.6, 2.8 Hz, 1H), 6.65 (d, J = 2.8 Hz, 1H), 5.00 (s, 2H), 4.00 (s, 1H), 2.79–2.74 (m, 2H), 2.30–2.14 (m, 3H), 1.82–1.78 (m, 2H), 1.58–1.53 (m, 3H), 1.50 (s, 3H), 1.40–1.35 (m, 1H), 1.23–1.17 (m, 5H), 0.90 (s, 3H). ^{13}C NMR (101 MHz, $CDCl_3$) δ 201.72, 157.15, 154.88, 143.64, 138.52, 137.73, 134.51, 131.36, 129.34, 128.77, 127.75, 126.63, 126.26, 125.95, 125.92, 120.84, 114.94, 112.27, 112.22, 79.39, 58.30, 55.68, 55.03, 44.35, 43.83, 40.62, 38.00, 31.97, 29.75, 29.71, 29.41, 22.73, 14.16, 13.65. HRESI-MS m/z calcd for $[M+H]^+$ $C_{39}H_{39}F_3N_2O_5$: 673.288400, found: 673.287550.

*5.1.5.3. 3-((((8S,9S,13S,14S,17S)-17-((R,E)-2-hydroxy-5-(4-(methylthio)phenyl)-3-oxopent-4-en-2-yl)-13-methyl-7,8,9,11,12,13,14,15,16,17-decahydro-6H cyclopenta[a]phenanthren-3-yl)oxy)methyl)-4-phenyl-1,2,5-oxadiazole 2-oxide **(20b)***. Yellowish white solid; 62% yield; ^{1}H NMR (600 MHz, $CDCl_3$) δ 7.81–7.76 (m, 2H), 7.72 (d, J = 15.5 Hz, 1H), 7.50–7.41 (m, 5H), 7.19–7.12 (m, 3H), 6.91 (d, J = 15.5 Hz, 1H), 6.72 (dd, J = 8.6, 2.8 Hz, 1H), 6.63 (d, J = 2.7 Hz, 1H), 4.98 (s, 2H), 4.14 (s, 1H), 2.84–2.67 (m, 2H), 2.43 (s, 3H), 2.31–2.10 (m, 3H), 1.84–1.74 (m, 2H), 1.62–1.49 (m, 3H), 1.47 (s, 3H), 1.39–1.33 (m, 1H), 1.30–1.12 (m, 5H), 0.89 (s, 3H). ^{13}C NMR (151 MHz, $CDCl_3$) δ 201.84, 157.16, 154.85, 145.21, 143.14, 138.59, 134.62, 131.37, 130.71, 129.36, 129.04, 127.78, 126.65, 126.27, 125.90, 117.26, 114.95, 112.28, 112.24, 79.11, 58.33, 55.70, 55.15, 44.30, 43.86, 40.65, 38.01, 29.77, 27.50, 26.62, 24.41, 23.66, 22.04,

15.09, 13.64. HRESI-MS *m/z* calcd for $[M+Na]^+$ $C_{39}H_{42}N_2O_5S$: 673.270664, found: 673.273272.

5.1.5.4. 3-((((8S,9S,13S,14S,17S)-17-((R,E)-5-(4-fluorophenyl)-2-hydroxy-3-oxopent-4-en-2-yl)-13-methyl-7,8,9,11,12,13,14,15,16,17-decahydro-6H-cyclopenta[a]phenanthren-3-yl)oxy)methyl)-4-phenyl-1,2,5-oxadiazole 2-oxide ***(20c)***. Yellowish white solid; 73% yield; ^{1}H NMR (600 MHz, $CDCl_3$) δ 7.78–7.75 (m, 2H), 7.71 (d, J = 15.6 Hz, 1H), 7.54–7.50 (m, 2H), 7.47–7.39 (m, 3H), 7.14 (d, J = 8.6 Hz, 1H), 7.04–6.99 (m, 2H), 6.90 (d, J = 15.6 Hz, 1H), 6.70 (dd, J = 8.6, 2.8 Hz, 1H), 6.62 (d, J = 2.8 Hz, 1H), 4.96 (s, 2H), 4.08 (s, 1H), 2.79–2.69 (m, 2H), 2.28–2.09 (m, 3H), 1.83–1.73 (m, 2H), 1.58–1.50 (m, 3H), 1.47 (s, 3H), 1.37–1.31 (m, 1H), 1.26–1.14 (m, 5H), 0.88 (s, 3H). ^{13}C NMR (151 MHz, $CDCl_3$) δ 201.79, 157.17, 154.88, 144.41, 138.57, 134.59, 131.38, 130.71, 130.65, 129.37, 127.78, 126.66, 126.27, 118.20, 116.31, 116.16, 114.96, 112.29, 112.25, 79.19, 58.34, 55.71, 55.10, 44.32, 43.86, 40.65, 38.01, 29.76, 27.51, 26.62, 24.37, 23.67, 22.07, 13.66. HRESI-MS *m/z* calcd for $[M+Na]^+$ $C_{38}H_{39}FN_2O_5$: 645.273521, found: 645.275728.

5.1.5.5. 3-((((8S,9S,13S,14S,17S)-17-((R,E)-2-hydroxy-5-(4-methoxyphenyl)-3-oxopent-4-en-2-yl)-13-methyl-7,8,9,11,12,13,14,15,16,17-decahydro-6H-cyclopenta[a]phenanthren-3-yl)oxy)methyl)-4-phenyl-1,2,5-oxadiazole 2-oxide ***(20d)***. White solid; 59% yield; ^{1}H NMR (400 MHz, $CDCl_3$) δ 7.89 (dd, J = 7.9, 1.4 Hz, 2H), 7.85 (d, J = 15.5 Hz, 1H), 7.63–7.54 (m, 5H), 7.27 (d, J = 15.5 Hz, 1H), 6.97 (d, J = 1.5 Hz, 2H), 6.94 (d, J = 8.5 Hz, 1H), 6.83 (dd, J = 8.5, 2.5 Hz, 1H), 6.74 (d, J = 2.5 Hz, 1H), 5.09 (s, 2H), 4.31 (s, 1H), 3.88 (s, 3H), 2.86 (q, J = 10.6 Hz, 2H), 2.36 (dd, J = 20.6, 7.9 Hz, 2H), 2.28–2.21 (m, 1H), 1.90 (dt, J = 8.5, 6.2 Hz, 2H), 1.69–1.63 (m, 3H), 1.58 (s, 3H), 1.47 (d, J = 10.2 Hz, 1H), 1.33 (dd, J = 17.1, 10.0 Hz, 5H), 1.00 (s, 3H). ^{13}C NMR (101 MHz, $CDCl_3$) δ 201.84, 162.04, 157.16, 154.84, 145.58, 138.59, 134.63, 131.37, 130.54, 129.36, 127.77, 127.01, 126.65, 126.25, 115.94, 114.93, 114.47, 112.24, 79.00, 58.30, 55.69, 55.48, 55.18, 44.26, 43.86, 40.65, 38.00, 29.76, 27.50, 26.62, 24.45, 23.66, 22.02, 13.62. HRESI-MS *m/z* calcd for $[M+H]^+$ $C_{39}H_{42}N_2O_6$: 635.311600, found: 635.310370.

5.1.5.6. 3-((((8S,9S,13S,14S,17S)-17-((R,E)-2-hydroxy-5-(5-methylthiophen-2-yl)-3-oxopent-4-en-2-yl)-13-methyl-7,8,9,11,12,13,14,15,16,17-decahydro-6H-cyclopenta[a]phenanthren-3-yl)oxy)methyl)-4-phenyl-1,2,5-oxadiazole 2-oxide ***(20e)***. Yellow solid; 45% yield; ^{1}H NMR (600 MHz, $CDCl_3$) δ 7.81–7.77 (m, 3H), 7.48–7.42 (m, 3H), 7.16 (d, J = 8.6 Hz, 1H), 7.09 (d, J = 3.6 Hz, 1H), 6.72 (dd, J = 8.6, 2.7 Hz, 1H), 6.68 (dd, J = 3.6, 1.0 Hz, 1H), 6.63 (d, J = 2.7 Hz, 1H), 6.58 (d, J = 15.2 Hz, 1H), 4.98 (s, 2H), 4.15 (s, 1H), 2.79–2.71 (m, 2H), 2.45 (s, 3H), 2.27–2.12 (m, 3H), 1.80–1.74 (m, 2H), 1.60–1.40 (m, 3H), 1.38–1.32 (m, 1H), 1.30–1.12 (m, 5H), 0.88 (s, 3H). ^{13}C NMR (151 MHz, $CDCl_3$) δ 201.58, 157.16, 154.85, 145.34, 138.60, 138.49, 137.82, 134.66, 133.69, 131.37, 129.36, 127.78, 127.03, 126.66, 126.27, 115.87, 114.94, 112.27, 112.24, 78.94, 58.32, 55.66, 55.20, 44.26, 43.84, 40.62, 38.01, 29.78, 27.50, 26.62, 24.44, 23.66, 22.03, 15.99, 13.61. HRESI-MS *m/z* calcd for $[M+Na]^+$ $C_{37}H_{40}N_2O_5S$: 647.255014, found: 647.256570.

5.1.5.7. 3-((((8S,9S,13S,14S,17S)-17-((R,E)-5-(5-bromothiophen-2-yl)-2-hydroxy-3-oxopent-4-en-2-yl)-13-methyl-7,8,9,11,12,13,14,15,16,17-decahydro-6H-cyclopenta[a]phenanthren-3-yl)oxy)methyl)-4-phenyl-1,2,5-oxadiazole 2-oxide ***(20f)***. Yellowish white solid; 72% yield; ^{1}H NMR (600 MHz, $CDCl_3$) δ 7.80–7.77 (m, 2H), 7.73 (d, J = 15.2 Hz, 1H), 7.49–7.42 (m, 3H), 7.16 (d, J = 8.6 Hz, 1H), 7.02 (d, J = 3.9 Hz, 1H), 6.98 (d, J = 3.9 Hz, 1H), 6.72 (dd, J = 8.6, 2.8 Hz, 1H), 6.64–6.61 (m, 2H), 4.99 (s, 2H), 4.03 (s, 1H), 2.81–2.71 (m, 2H), 2.27–2.11 (m, 3H), 1.81–1.72 (m, 2H), 1.60–1.51 (m, 3H), 1.44 (s, 3H), 1.38–1.33 (m, 1H), 1.29–1.12 (m, 5H), 0.88 (s, 3H). ^{13}C NMR (151 MHz, $CDCl_3$) δ 201.43, 157.16, 154.85, 141.33, 138.57, 137.05, 134.60, 133.00, 131.44, 131.37, 129.36, 127.78, 126.66, 126.27, 117.54, 117.12, 114.94, 112.28, 112.24, 79.12, 58.32, 55.64, 55.11, 44.30, 43.82, 40.60, 38.01, 29.77, 27.49, 26.61, 24.34, 23.65, 22.05, 13.62. HRESI-MS *m/z* calcd for $[M+Na]^+$ $C_{36}H_{37}BrN_2O_5S$: 711.149876, found: 711.153027.

5.1.5.8. 3-((((8S,9S,13S,14S,17S)-17-((R,E)-5-(5-bromofuran-2-yl)-2-hydroxy-3-oxopent-4-en-2-yl)-13-methyl-7,8,9,11,12,13,14,15,16,17-decahydro-6H-cyclopenta[a]phenanthren-3-yl)oxy)methyl)-4-phenyl-1,2,5-oxadiazole 2-oxide ***(20g)***. Brown solid; 65% yield; ^{1}H NMR (600 MHz, $CDCl_3$) δ 7.78–7.74 (m, 2H), 7.46–7.40 (m, 3H), 7.36 (d, J = 15.2 Hz, 1H), 7.14 (d, J = 8.6 Hz, 1H), 6.80 (d, J = 15.2 Hz, 1H), 6.70 (dd, J = 8.6, 2.6 Hz, 1H), 6.62 (d, J = 2.6 Hz, 1H), 6.57 (d, J = 3.5 Hz, 1H), 6.36 (d, J = 3.5 Hz, 1H), 4.96 (s, 2H), 4.07 (s, 1H), 2.78–2.69 (m, 2H), 2.25–2.11 (m, 3H), 1.81–1.73 (m, 2H), 1.57–1.47 (m, 3H), 1.44 (s, 3H), 1.34–1.30 (m, 1H), 1.27–1.11 (m, 5H), 0.86 (s, 3H). ^{13}C NMR (151 MHz, $CDCl_3$) δ 201.62, 157.16, 154.87, 153.05, 138.56, 134.64, 131.38, 130.09, 129.37, 127.78, 126.68, 126.42, 126.28, 119.17, 116.39, 114.94, 114.84, 112.29, 112.25, 79.18, 58.33, 55.62, 54.92, 44.31, 43.83, 40.55, 38.02, 29.78, 27.52, 26.63, 24.31, 23.69, 22.05, 13.66. HRESI-MS *m/z* calcd for $[M+Na]^+$ $C_{36}H_{37}BrN_2O_6$: 695.172720, found: 695.175669.

5.1.5.9. 3-((((8S,9S,13S,14S,17S)-17-((S,E)-2-hydroxy-5-(4-methoxyphenyl)-3-oxopent-4-en-2-yl)-13-methyl-7,8,9,11,12,13,14,15,16,17-decahydro-6H-cyclopenta[a]phenanthren-3-yl)oxy)methyl)-4-phenyl-1,2,5-oxadiazole 2-oxide ***(23a)***. Yellow solid; 39% yield; ^{1}H NMR (600 MHz, $CDCl_3$) δ 7.79–7.76 (m, 2H), 7.75 (d, J = 11.0 Hz, 1H), 7.52 (d, J = 8.7 Hz, 2H), 7.48–7.41 (m, 3H), 7.04 (d, J = 8.6 Hz, 1H), 6.89–6.85 (m, 3H), 6.66 (dd, J = 8.6, 2.5 Hz, 1H), 6.62 (d, J = 2.5 Hz, 1H), 4.96 (s, 2H), 3.89 (s, 1H), 3.79 (s, 3H), 2.79–2.72 (m, 2H), 2.10–1.98 (m, 3H), 1.90–180 (m, 2H), 1.72–1.48 (m, 3H), 1.31 (s, 3H), 1.27–1.13 (m, 6H), 0.70 (s, 3H). ^{13}C NMR (151 MHz, $CDCl_3$) δ 202.76, 162.02, 157.15, 154.80, 144.19, 138.53, 134.57, 131.34, 130.47, 129.34, 127.76, 127.16, 126.61, 126.25, 117.71, 114.87, 114.54, 112.24, 112.21, 79.05, 58.28, 56.35, 55.59, 55.50, 43.70, 43.02, 39.16, 37.85, 29.79, 27.51, 26.51, 26.27, 22.89, 22.66, 13.32. HRESI-MS *m/z* calcd for $[M+H]^+$ $C_{39}H_{42}N_2O_6$: 635.311564, found: 635.313847.

5.1.5.10. 3-((((8S,9S,13S,14S,17S)-17-((S,E)-2-hydroxy-3-oxo-5-(4-(trifluoromethyl)phenyl)pent-4-en-2-yl)-13-methyl-7,8,9,11,12,13,14,15,16,17-decahydro-6H-cyclopenta[a]phenanthren-3-yl)oxy)methyl)-4-phenyl-1,2,5-oxadiazole 2-oxide ***(23b)***. Yellow solid; 34% yield; ^{1}H NMR (600 MHz, $CDCl_3$) δ 7.78 (m, 3H), 7.53 (d, J = 8.1 Hz, 2H), 7.50–7.39 (m, 8H), 7.07 (d, J = 8.6 Hz, 1H), 6.77 (d, J = 15.8 Hz, 1H), 6.68 (dd, J = 8.6, 2.4 Hz, 1H), 6.64 (d, J = 2.4 Hz, 1H), 6.33 (d, J = 15.8 Hz, 1H), 4.97 (s, 2H), 4.34 (s, 1H), 2.79–2.74 (m, 2H), 2.11–2.03 (m, 2H), 1.95–1.90 (m, 2H), 1.84–1.78 (m, 2H), 1.64–1.62 (d, 1H), 1.52–150 (m, 1H), 1.46 (s, 3H), 1.42–1.22 (m, 6H), 0.76 (s, 3H). ^{13}C NMR (151 MHz, $CDCl_3$) δ 212.98, 157.14, 154.91, 138.34, 134.02, 131.66, 131.37, 129.86, 129.35, 127.76, 126.85, 126.76, 126.69, 126.24, 125.74, 125.72, 114.90, 112.36, 112.20, 79.70, 58.29, 56.18, 55.80, 47.32, 43.52, 39.64, 38.50, 29.70, 28.93, 27.74, 26.54, 25.08, 24.84, 13.78. HRESI-MS *m/z* calcd for $[M+Na]^+$ $C_{39}H_{39}F_3N_2O_5$: 695.270328, found: 695.272678.

5.1.5.11. 3-((((8S,9S,13S,14S)-17-((R)-2-hydroxy-3-oxobutan-2-yl)-13-methyl-7,8,9,11,12,13,14,15,16,17-decahydro-6H-cyclopenta[a]phenanthren-3-yl)oxy)methyl)-4-phenyl-1,2,5-oxadiazole 2-oxide ***(25)***. ^{1}H NMR (400 MHz, $CDCl_3$) δ 7.85 (dd, J = 8.0, 1.6 Hz, 2H), 7.56–7.48 (m, 3H), 7.22 (d, J = 8.6 Hz, 1H), 6.78 (dd, J = 8.6, 2.7 Hz, 1H), 6.71 (d, J = 2.7 Hz, 1H), 5.05 (s, 2H), 3.99 (s, 1H), 2.88–2.80 (m, 2H), 2.32–2.20 (m, 6H), 1.89–1.79 (m, 2H), 1.57 (m, 3H), 1.47 (s, 3H), 1.34–1.23 (m, 6H), 0.92 (s, 3H). ^{13}C NMR (101 MHz, $CDCl_3$) δ 211.83, 157.16, 154.88,

138.53, 134.54, 131.39, 129.37, 127.76, 126.65, 126.25, 114.94, 112.28, 80.14, 58.32, 55.67, 55.10, 44.20, 43.80, 40.59, 37.96, 29.77, 27.52, 26.59, 24.63, 23.73, 23.35, 22.11, 13.53. ^{13}C DEPT-NMR (101 MHz, $CDCl_3$) δ 131.45, 129.36, 127.76, 126.64, 114.93, 112.28, 58.31 (inverted), 55.72, 55.15, 43.80 (inverted), 40.66, 37.97, 37.95 (inverted), 29.76 (inverted), 27.50, 26.57 (inverted), 24.62, 23.70 (inverted), 23.33, 22.09 (inverted).

*5.1.6. General procedure for preparing of (R)-3-((8S,9S,13S,14S,17S)-3-(allyloxy)-13-methyl-7,8,9,11,12,13,14,15,16,17-decahydro-6H-cyclopenta[a]phenanthren-17-yl)-3-hydroxybutan-2-one **(26)***

To a stirred solution of phenolic derivative **24** (0.2066 g, 0.37 mmol) in THF (2 mL), allyl bromide (0.0895, 0.74 mmol) and NaOH (0.0296 g, 0.74 mmol) were added. The reaction mixture was heated under reflux at 80 °C for 2 h (as indicated by TLC). After completion, water (15 mL) was added and the reaction mixture was extracted with ethyl acetate (3 × 10 mL), washed with brine, dried over anhydrous sodium sulphate, filtered and evaporated under *vaccu* (80 °C) to afford 3-allyloxy-estrone derivative **26** [65–67].

White solid; 85% yield; ^{1}H NMR (400 MHz, $CDCl_3$) δ 7.11 (d, J = 8.6 Hz, 1H), 6.65 (dd, J = 8.6, 2.5 Hz, 1H), 6.57 (d, J = 2.5 Hz, 1H), 5.98 (ddt, J = 17.2, 10.5, 5.3 Hz, 1H), 5.33 (dd, J = 17.2, 1.6 Hz, 1H), 5.19 (dd, J = 10.5, 1.6 Hz, 1H), 4.50–4.36 (m, 2H), 3.91 (s, 1H), 2.88–2.69 (m, 2H), 2.24–2.19 (m, 2H), 2.16 (s, 3H), 1.82–1.71 (m, 2H), 1.64–1.47 (m, 3H), 1.40 (s, 3H), 1.35–1.16 (m, 7H), 0.85 (s, 3H). ^{13}C NMR (101 MHz, $CDCl_3$) δ 211.80, 156.49, 137.95, 133.60, 132.83, 126.20, 117.46, 114.71, 112.22, 80.13, 68.80, 55.72, 55.11, 44.24, 43.82, 40.67, 38.06, 29.81, 27.63, 26.59, 24.61, 23.70, 23.32 ($COCH_3$), 22.09, 13.51.

*5.1.7. General procedure for preparing of (3R)-3-((8S,9S,13S,14S,17S)-3-(2,3-diiodopropoxy)-13-methyl-7,8,9,11,12,13,14,15,16,17-decahydro-6H-cyclopenta[a]phenanthren-17-yl)-3-hydroxybutan-2-one **(27)***

Iodine (0.95 g, 0.373 mmol) was added in one portion to a stirred solution of 3-allyloxy derivative **26** (0.1427 g, 0.373 mmol) and $AgNO_3$ (0.190 g, 1.120 mmol) in CH_3CN (2.5 mL). The reaction mixture was stirred at room temperature for 30 min, then filtered, diluted with distilled water (7.5 mL), and extracted with EtOAc (3 × 10 mL). The combined organic layers were washed with distilled water, brine, dried over anhydrous Na_2SO_4 and evaporated under *vaccu*. The resulting yellow oil was purified by flash chromatography (Hexane/EtOAc, 8:2) to yield the title product as a yellow oily diastereomeric mixture in the ratio about 1:1 (NMR detection) [67,68].

Yellow oil; 86% yield; ^{1}H NMR (600 MHz, $CDCl_3$) δ 7.13 (d, J = 8.5 Hz, 1H), 6.63 (dd, J = 8.5, 2.6 Hz, 1H), 6.55 (d, J = 2.6 Hz, 1H), 4.77 (dd, J = 6.4, 2.6 Hz, 1H), 4.23–4.18, 4.17–4.09 (two m, 2H), 3.91 (s, 1H), 3.45, 3.37 (two dd, J = 10.8, 6.4, 10.8, 5.3 Hz, 2H), 2.79–2.71 (m, 2H), 2.24–2.18 (m, 2H), 2.16 (s, 3H), 1.82–1.72 (m, 2H), 1.65–1.59 (m, 1H), 1.51–1.46 (m, 3H), 1.40 (s, 3H), 1.36–1.14 (m, 6H), 0.85 (s, 3H). ^{13}C NMR (151 MHz, $CDCl_3$) δ 213.08, 156.96, 156.79, 139.65, 139.63, 135.29, 127.78, 127.77, 116.11, 116.00, 113.40, 113.37, 81.42, 81.26, 74.87, 67.96, 56.98, 56.40, 45.51, 45.09, 41.91, 39.29, 31.07, 28.84, 27.89, 25.91, 25.00, 24.63, 23.39, 20.94, 14.81.

*5.1.8. General procedure for preparing of 3-(((8S,9S,13S,14S,17S)-17-((R)-2-hydroxy-3-oxobutan-2-yl)-13-methyl-7,8,9,11,12,13,14,15,16,17-decahydro-6H-cyclopenta[a]phenanthren-3-yl)oxy)propane-1,2-diyl dinitrate **(28)***

To a stirred solution of diiodo derivative **27** (0.2374 g, 0.373 mmol) in CH_3CN (2.5 mL), $AgNO_3$ (0.190 g, 1.120 mmol) in CH_3CN (2.5 mL) was added. The reaction mixture was stirred at room temperature for 1 h, then refluxed for 17 h (as indicated by TLC). After cooling, the mixture was filtered, diluted with distilled water (7.5 mL), and extracted with EtOAc (3 × 10 mL). The combined organic layers were washed with distilled water, brine, dried and evaporated. The resulting yellow oil was partly purified by flash chromatography (Hexane/EtOAc, 8:2) to yield the title product as a yellow oily diastereomeric mixture in the ratio about 1:0.5 (NMR detection) [67,68].

Yellow oil; 37% yield; ^{1}H NMR (400 MHz, $CDCl_3$) δ 7.15 (d, J = 8.7 Hz, 1H), 6.62 (dd, J = 8.7, 2.5 Hz, 1H), 6.55 (d, J = 2.5 Hz, 1H), 5.62–5.47 (m, 1H), 4.85, 4.70 (two dd, J = 12.9, 3.3, 12.9, 6.6 Hz, 2H), 4.21–4.09 (m, 2H), 3.92 (s, 1H), 2.80–2.73 (m, 2H), 2.27–2.18 (m, 3H), 2.16 (s, 3H), 1.83–1.73 (m, 2H), 1.65–1.47 (m, 3H), 1.40 (s, 3H), 1.35–1.14 (m, 6H), 0.86 (s, 3H). ^{13}C NMR (151 MHz, $CDCl_3$) δ 211.76, 211.71, 155.44, 154.02, 138.78, 138.43, 136.81, 136.55, 134.29, 126.55, 114.59, 113.01, 111.99, 111.95, 82.96, 80.11, 80.07, 69.13, 68.97, 65.95, 65.93, 64.72, 55.67, 55.54, 55.11, 55.05, 44.20, 44.14, 43.78, 43.48, 40.60, 40.44, 37.98, 37.70, 31.96, 29.76, 29.73, 29.69, 29.60, 27.51, 27.29, 26.59, 26.55, 24.61, 23.68, 23.29, 22.72, 22.08, 14.16, 13.47.

*5.1.9. General procedure for preparing of 3-(((8S,9S,13S,14S,17S)-17-((R,E)-2-hydroxy-3-oxo-5-(4-(trifluoromethyl)phenyl)pent-4-en-2-yl)-13-methyl-7,8,9,11,12,13,14,15,16,17-decahydro-6H-cyclopenta[a]phenanthren-3-yl)oxy)propane-1,2-diyl dinitrate **(29)***

To a solution of α-hydroxy methyl ketone **28** (0.1836 g, 0.4 mmol) in THF (1 mL) in an open 20 mL-glass vial, 4-(trifluoromethyl)benzaldehyde (0.8 mmol) and sodium hydroxide (0.0464 g, 1.16 mmol) were added at room temperature and the reaction mixture was then heated at 105 °C for 10 min with continuing addition of THF by an approximate rate of 0.5 mL/min (avoid dryness). The reaction mixture was then quenched by the addition of water (15 mL), followed by extraction with EtOAc (3 × 20 mL), washed with brine, dried over anhydrous Na_2SO_4, and concentrated in *vacuo* [37,62–64]. The resulting yellow oil was purified by flash chromatography (Hexane/EtOAc, 8:2) to yield the title product NO-CIEA **29** in 44%.

Yellow solid; ^{1}H NMR (600 MHz, $CDCl_3$) δ 7.75 (d, J = 15.5 Hz, 1H), 7.63 (d, J = 8.6 Hz, 2H), 7.59 (d, J = 8.6 Hz, 2H), 7.14 (d, J = 8.6 Hz, 1H), 7.04 (d, J = 15.5 Hz, 1H), 6.62 (dd, J = 8.6, 2.5 Hz, 1H), 6.54 (d, J = 2.5 Hz, 1H), 5.53–5.46 (m, 1H), 4.83, 4.69 (two dd, J = 12.9, 3.3, 12.9, 6.6 Hz, 2H), 4.15–4.13, 4.12–4.10 (two m, 2H), 4.00 (s, 1H), 2.80–2.69 (m, 2H), 2.30–2.05 (m, 3H), 2.03–1.86 (m, 1H), 1.82–1.79 (m, 2H), 1.61–1.51 (m, 3H), 1.49 (s, 3H), 1.36–1.15 (m, 5H), 0.89 (s, 3H). ^{13}C NMR (151 MHz, $CDCl_3$) δ 201.72, 155.45, 143.67, 138.46, 137.68, 134.29, 128.77, 128.73, 126.56, 125.95, 120.81, 114.61, 111.96, 79.38, 68.96, 64.70, 55.67, 55.04, 44.36, 43.81, 40.63, 38.02, 29.75, 27.50, 26.62, 26.28, 24.27, 23.65, 22.07, 13.65. HRESI-MS *m/z* calcd for $[M+H]^+$ $C_{33}H_{38}F_3N_2O_9$: 663.252392, found: 663.255249.

*5.1.10. General procedure for preparing of (R,E)-2-((8S,9S,13S,14S,17S)-3-(allyloxy)-13-methyl-7,8,9,11,12,13,14,15,16,17-decahydro-6H-cyclopenta[a]phenanthren-17-yl)-2,6-dihydroxy-6-methylhept-4-en-3-one **(31)***

To a stirred solution of α-hydroxy methyl ketone **27** (0.500 g, 0.79 mmol) in THF (1.6 mL), LDA (1.42 mL, 2.83 mmol, 2 M in THF) was added at −78 °C and stirred for 1 h. A solution of 2-((*tert*-butyldimethylsilyl)oxy)-2-methylpropanal **11** (0.3997 g, 1.98 mmol) in THF (5.3 mL) was then added at −78 °C and the reaction mixture was allowed to slowly warm to room temperature and stirred for 20 h. The reaction mixture was then quenched by the addition of saturated NH_4Cl (20 mL), extracted with EtOAc (3 × 50 mL), dried over anhydrous Na_2SO_4, and concentrated in *vacuo* [37,63]. The crude product was purified by silica gel column chromatography with hexanes/EtOAc (9.5:0.5) to yield compounds **26** and **31**.

31; White solid; 25% yield; ^{1}H NMR (600 MHz, $CDCl_3$) δ 7.07 (d, J = 8.6 Hz, 1H), 7.03 (d, J = 15.2 Hz, 1H), 6.60 (dd, J = 8.6, 2.7 Hz, 1H), 6.57 (d, J = 15.2 Hz, 1H), 6.52 (d, J = 2.7 Hz, 1H), 5.93 (ddt, J = 17.2, 10.6, 5.3 Hz, 1H), 5.28 (dd, J = 17.2, 1.6 Hz, 1H), 5.15 (dd, J = 10.5, 1.6 Hz, 1H), 4.39 (dt, J = 5.3, 1.6 Hz, 2H), 4.00 (s, 1H), 2.77–2.66 (m, 2H), 2.21–2.05 (m, 3H), 1.76–1.68 (m, 2H), 1.58 (s, 1H), 1.56–1.53 (m, 1H), 1.48–1.41 (m, 3H), 1.37 (s, 3H), 1.29 (s, 6H),

1.24–1.07 (m, 5H), 0.82 (s, 3H). ^{13}C NMR (151 MHz, $CDCl_3$) δ 202.37, 156.47, 156.00 (CO-CH=*C*H), 137.97, 133.62, 132.90, 126.23, 118.10 (CO-*C*H=CH), 117.47, 114.72, 112.22, 79.20, 71.37 (*C*24-OH), 68.81, 55.66, 54.62, 44.32, 43.84, 40.60, 38.10, 29.83, 29.57 (C25 & C26), 27.63, 26.62, 24.17, 23.67, 21.98, 13.65. ^{13}C DEPT-NMR (151 MHz, $CDCl_3$) δ 156.01, 133.62, 126.23, 118.10, 117.47 (inverted *C*H_2), 114.73, 112.23, 68.81 (inverted *C*H_2), 55.66, 54.63, 43.84, 40.60 (inverted *C*H_2), 38.10, 29.83 (inverted *C*H_2), 29.56, 27.63 (inverted *C*H_2), 26.62 (inverted *C*H_2), 24.17, 23.67 (inverted *C*H_2), 21.99 (inverted *C*H_2), 13.66.

6. Biological evaluation

6.1. In vitro cytotoxicity assay

The in vitro antiproliferation of the chemical compounds was measured by the MTT reagent, as described in the literature [42–44]. Briefly, 2×10^4 HepG2 cells in 100 µL of medium per well were seeded in 96-well plates. After cultured for 24 h in 37 °C humidified incubator (5% CO_2), cells were incubated in complete mediums with the Erlotinib (as a reference drug), absence (negative control) and presence of various concentrations of tested compounds, respectively, for 48 h. Each group was arranged four parallel wells. MTT solution (20 µL; 5 mg/mL) was added to each well and incubated at 37 °C for 2 h. Last, the MTT-containing medium was discarded and 200 µL of DMSO per well was added and mixed well to dissolve the formazan crystals newly formed. Absorbance of each well was determined by a microplate reader (Hidex Sense) at a 570 nm wavelength. Survival percentage was calculated using the following equation:

$$\text{Inhibitory rate } \% = (Abs_{570\ \text{control cells}} - Abs_{570\ \text{treated cells}})/Abs_{570\ \text{control cells}} \times 100.$$

IC_{50} values were obtained from linear regression analysis of the concentration-response curves plotted for each tested compound.

6.2. Measurement of Intracellular NO

The intracellular level of NO after compounds treatment was quantified using the NO-sensitive fluorophore DAF-FM DA. HepG2 cells were seeded in a six-well plate at $7.5x10^5$ cells per well and allowed to grow overnight. Cells were loaded with 2 mL of 2.5 µM DAF-FM DA in HBSS in each well at 37 °C and 5% CO_2. After 30 min of incubation, the cells were rinsed with HBSS two times to remove excess of probe. The compounds were dissolved in DMSO and different concentrations were prepared and added to the cells. After 1, 6, 12 and 24 h of incubation, cells were washed with HPSS, trypsinized and pipetted into flow cytometer test tubes. The fluorescence of the benzotriazole derivative formed on DAF-FM DA's reaction with NO was analyzed by flow cytometer (BD Acuuri C6, Becton-Dickinson, Mountain View, CA) with the excitation source at 495 nm and emission at 515 nm. Data are expressed as mean values of at least two runs ± the standard deviation (SD) [43,50–52].

6.3. Cell cycle analysis

The cells were seeded as 2.5×10^5 cells/mL in a 6-well plate (2 mL/well) and allowed to adhere overnight at 37 °C and 5% CO_2. The cells were incubated with NO-CIEA **17** (4.69 µM), **20a** (12.5 µM) and DMSO (0.001%) as a control for 24 h. The cells were washed twice with ice-cold 1X PBS (Hyclone™ Laboratories, Inc) and collected after trypsinization [69]. The cell pellet was washed two times with ice-cold 1X PBS and fixed with ice-cold 70% ethanol overnight at −20 °C. After that, the cells were washed once with ice-cold PBS and the second wash with ice-cold PBS-2% FBS. The cell pellet was re-suspended in 500 µL propidium iodide (PI)/RNase staining solution (BD Biosciences) and 0.1% triton x-100 for 30 min at room temperature in the dark and analyzed within 1 h by flow cytometer (BD Accuri C6, Becton-Dickinson, Mountain View, CA). Data was analyzed by MFLT32 software and 10,000 events with slow flow rate were recorded for each sample [32,70].

6.4. In-cell western assay (ICW)

HepG2 Cell line were seeded into clear bottomed and black walled 96-well plates with a density of 0.5×10^6 cells per mL and allowed to grow to confluence. The next day, cells were treated with different concentrations of NO-CIEA **17** (1.2, 2.4 and 4.8 µM) for 24 h and DMSO was used as a control. Cells were then fixed with 3.7% formaldehyde in 1X PBS for 30 min and then washed and permeabilized with 0.1% TritonX-100 in 1X PBS. Cells were then blocked with 1X PBS fish gel solution and then incubated with an antibody to EGFR (cell signaling technology), Phospho-EGFR (Santa Cruz Biotechnology), MAPK (Erk1/2; Santa Cruz Biotechnology), Phospho-MAPK (p-Erk1/2; Santa Cruz Biotechnology), Phospho-MEK1/2 (Cell Signaling Technology), β-actin (Invitrogen, Thermo Fisher Scientific), MRP2 (Abcam) and GAPDH (Santa Cruz Biotechnology) for 2 h with gentle shaking then incubated overnight at 4 °C without shaking (i.e: stationary). Cells were then washed with 0.1% Tween-20 in 1X PBS four times and then incubated with secondary antibodies conjugated to IRdye for 1 h with gentle shaking (protect from light). Cells were then washed with 0.1% Tween-20 in 1X PBS four times. After the last wash, any residual liquid was gently pipetted out and the plate was blotted dry using the In-cell western protocol on an Odyssey® imager (LI-COR®) according to manufacturer s directions [53–57]. Phospho-proteins were normalized for total protein signals while p-MEK1/2 and MRP2 were normalized for the β-actin and GAPDH loading controls, respectively, to correct for well-to-well variation in cell number and percent-inhibition determined relative to control wells. Data are expressed as mean values of at least two runs ± the standard deviation (SD).

6.5. Docking studies

This was done using OpenEye® molecular Modeling software. A virtual library of structurally modified NO-CIEAs were energy minimized using MMFF94 force field, followed by generation of multi-conformers using OMEGA® application. The whole energy minimized library will be docked along with the prepared EGFR (PDB code: 1M17) or ERK (PDB code: 2OJJ) using FRED® application to generate a physical property (ΔG) reflecting the predicted energy profile of ligand-receptor complex. Vida® application can be employed as a visualization tool to show the potential binding interactions of the ligands to the receptor of interest [32,61,71–73].

Acknowledgments

We wish to acknowledge the Egyptian government for financial support via the Egyptian Ministry of Higher Education and Scientific Research. We are also grateful to OpenEye® molecular modeling software for supporting an academic license.

References

[1] F. Bellissimo, M.R. Pinzone, B. Cacopardo, G. Nunnari, Diagnostic and therapeutic management of hepatocellular carcinoma, World J. Gastroenterol. 21 (2015) 12003–12021.
[2] D. Chen, C.K. Soh, W.H. Goh, H. Wang, Design, synthesis, and preclinical evaluation of fused pyrimidine-based hydroxamates for the treatment of hepatocellular carcinoma, J. Med. Chem. 61 (2018) 1552–1575.
[3] National Cancer Institute, Cancer stat facts: Liver and intrahepatic bile duct cancer. https://seer.cancer.gov/statfacts/html/livibd.html, 2018 (accessed April 2018).
[4] Y.A. Ghouri, I. Mian, J.H. Rowe, Review of hepatocellular carcinoma: epidemiology, etiology, and carcinogenesis, J. Carcinogenesis 16 (2017) 1.
[5] D.H. Ziada, S. El Sadany, H. Soliman, S. Abd-Elsalam, M. Salama, N. Hawash, A. Selim, M. Hamisa, H.M. Elsabagh, Prevalence of hepatocellular carcinoma in

chronic hepatitis C patients in mid delta, Egypt: a single center study, J. Egyptian Natl. Cancer Inst. 28 (2016) 257–262.
[6] M.S. Grandhi, A.K. Kim, S.M. Ronnekleiv-Kelly, I.R. Kamel, M.A. Ghasebeh, T.M. Pawlik, Hepatocellular carcinoma: from diagnosis to treatment, Surgical Oncol. 25 (2016) 74–85.
[7] I.O. Ng, C.L. Liu, S.T. Fan, M. Ng, Expression of P-glycoprotein in hepatocellular carcinoma, Am. J. Clin. Pathol. 113 (2000) 355–363.
[8] J.-G. Park, S.-K. Lee, I.-G. Hong, H.-S. Kim, K.-H. Lim, K.-J. Choe, W.-H. Kim, Y.-I. Kim, T. Tsuruo, M.M. Gottesman, MDR1 gene expression: its effect on drug resistance to doxorubicin in human hepatocellular carcinoma cell lines, J. Natl. Cancer Inst. 86 (1994) 700–705.
[9] S. Ma, C.C.-H. Ma, Recent developments in the effects of nitric oxide-donating statins on cardiovascular disease through regulation of tetrahydrobiopterin and nitric oxide, Vascular Pharmacol. 63 (2014) 63–70.
[10] N. Tuteja, M. Chandra, R. Tuteja, M.K. Misra, Nitric oxide as a unique bioactive signaling messenger in physiology and pathophysiology, BioMed Res. Int. 2004 (2004) 227–237.
[11] X.-Y. Jin, S.-Y. Fan, H.-W. Li, W.-G. Shi, W. Chen, H.-F. Wang, B.-H. Zhong, Novel liver-specific nitric oxide (NO) releasing drugs with bile acid as both NO carrier and targeting ligand, Chinese Chem. Lett. 25 (2014) 787–790.
[12] K. Kashfi, M. Chattopadhyay, R. Kodela, NOSH-sulindac (AVT-18A) is a novel nitric oxide- and hydrogen sulfide-releasing hybrid that is gastrointestinal safe and has potent anti-inflammatory, analgesic, antipyretic, anti-platelet, and anti-cancer properties, Redox Biol. 6 (2015) 287–296.
[13] F. Vannini, A.C. MacKessack-Leitch, E.K. Eschbach, M. Chattopadhyay, R. Kodela, K. Kashfi, Synthesis and anti-cancer potential of the positional isomers of NOSH-aspirin (NBS-1120) a dual nitric oxide and hydrogen sulfide releasing hybrid, Bioorganic Med. Chem. Lett. 25 (2015) 4677–4682.
[14] M. Klink, M. Kielbik, I.S. Kielbik, P. Przygodzka, Z. Sulowska, Antitumoral activity of nitric oxide-releasing compounds, Redox Biol. 5 (2015) 420.
[15] R. González, Á.J. De la Rosa, S. Romero-Brufau, L. Barrera-Pulido, F. Gallardo-Chamizo, S. Pereira, L.M. Marín, J.M. Álamo, Á. Rodríguez-Hernández, F.J. Padillo, J. Muntané, Nitric oxide synthase type III overexpression by gene therapy exerts antitumoral activity in mouse hepatocellular carcinoma, Redox Biol. 5 (2015) 420–421.
[16] K. Sharma, H. Chakrapani, Site-directed delivery of nitric oxide to cancers, Nitric Oxide 43 (2014) 8–16.
[17] V.V.S. Rajendra Prasad, G. Deepak Reddy, I. Kathmann, M. Amareswararao, G.J. Peters, Nitric oxide releasing acridone carboxamide derivatives as reverters of doxorubicin resistance in MCF7/Dx cancer cells, Bioorganic Chem. 64 (2016) 51–58.
[18] X. Tang, X. Gu, H. Ai, G. Wang, H. Peng, Y. Lai, Y. Zhang, Synthesis and evaluation of nitric oxide-releasing DDB derivatives as potential Pgp-mediated MDR reversal agents in MCF-7/Adr cells, Bioorganic Med. Chem. Lett. 22 (2012) 801–805.
[19] S. Fiorucci, E. Antonelli, E. Distrutti, A. Mencarelli, S. Farneti, P.D. Soldato, A. Morelli, Liver delivery of NO by NCX-1000 protects against acute liver failure and mitochondrial dysfunction induced by APAP in mice, British J. Pharmacol. 143 (2004) 33–42.
[20] J. Cicenas, K. Kalyan, A. Sorokinas, E. Stankunas, J. Levy, I. Meskinyte, V. Stankevicius, A. Kaupinis, M. Valius, Roscovitine in cancer and other diseases, Ann. Transl. Med. 3 (2015) 135–146.
[21] H.S. Khalil, V. Mitev, T. Vlaykova, L. Cavicchi, N. Zhelev, Discovery and development of Seliciclib. How systems biology approaches can lead to better drug performance, J. Biotechnol. 202 (2015) 40–49.
[22] A.A. Alghasham, Cucurbitacins–a promising target for cancer therapy, Int. J. Health Sci. 7 (2013) 77–89.
[23] M.S. Ahmed, F.T. Halaweish, Cucurbitacins: potential candidates targeting mitogen-activated protein kinase pathway for treatment of melanoma, J. Enzyme Inhibition Med. Chem. 29 (2014) 162–167.
[24] D.H. Lee, G.B. Iwanski, N.H. Thoennissen, Cucurbitacin: ancient compound shedding new light on cancer treatment, Sci. World J. 10 (2010) 413–418.
[25] J. Bartalis, F.T. Halaweish, In vitro and QSAR studies of cucurbitacins on HepG2 and HSC-T6 liver cell lines, Bioorganic Med. Chem. 19 (2011) 2757–2766.
[26] L.C. Kopel, M.S. Ahmed, F.T. Halaweish, Synthesis of novel estrone analogs by incorporation of thiophenols via conjugate addition to an enone side chain, Steroids 78 (2013) 1119–1125.
[27] P.V. Korita, T. Wakai, Y. Shirai, Y. Matsuda, J. Sakata, M. Takamura, M. Yano, A. Sanpei, Y. Aoyagi, K. Hatakeyama, Y. Ajioka, Multidrug resistance-associated protein 2 determines the efficacy of cisplatin in patients with hepatocellular carcinoma, Oncol. Rep. 23 (2010) 965–972.
[28] M. Buchler, J. Konig, M. Brom, J. Kartenbeck, H. Spring, T. Horie, D. Keppler, cDNA cloning of the hepatocyte canalicular isoform of the multidrug resistance protein, cMrp, reveals a novel conjugate export pump deficient in hyperbilirubinemic mutant rats, J. Biol. Chem. 271 (1996) 15091–15098.
[29] K. Sodani, A. Patel, R.J. Kathawala, Z.S. Chen, Multidrug resistance associated proteins in multidrug resistance, Chinese J. Cancer 31 (2012) 58–72.
[30] Y. Cui, J. Konig, J.K. Buchholz, H. Spring, I. Leier, D. Keppler, Drug resistance and ATP-dependent conjugate transport mediated by the apical multidrug resistance protein, MRP2, permanently expressed in human and canine cells, Mol. Pharmacol. 55 (1999) 929–937.
[31] S. Elgazwi, Study of anti-proliferative activity of cucurbitacins inspired estrone analogs on hepatocellular carcinoma, Chemistry and Biochemistry, South Dakota State University, South Dakota, 2018, p. 145.
[32] Y.A.M.M. Elshaier, M.A. Shaaban, M.K. Abd El Hamid, M.H. Abdelrahman, M.A. Abou-Salim, S.M. Elgazwi, F. Halaweish, Design and synthesis of pyrazolo[3,4-d]pyrimidines: nitric oxide releasing compounds targeting hepatocellular carcinoma, Bioorganic Med. Chem. 25 (2017) 2956–2970.
[33] V.C. Jordan, S. Mittal, B. Gosden, R. Koch, M.E. Lieberman, Structure-activity relationships of estrogens, Environ. Health Perspect. 61 (1985) 97–110.
[34] J. Stamos, M.X. Sliwkowski, C. Eigenbrot, Structure of the epidermal growth factor receptor kinase domain alone and in complex with a 4-anilinoquinazoline inhibitor, J. Biol. Chem. 277 (2002) 46265–46272.
[35] A.M. Aronov, C. Baker, G.W. Bemis, J. Cao, G. Chen, P.J. Ford, U.A. Germann, J. Green, M.R. Hale, M. Jacobs, J.W. Janetka, F. Maltais, G. Martinez-Botella, M.N. Namchuk, J. Straub, Q. Tang, X. Xie, Flipped out: structure-guided design of selective pyrazolylpyrrole ERK inhibitors, J. Med. Chem. 50 (2007) 1280–1287.
[36] S. Korde Choudhari, M. Chaudhary, S. Bagde, A.R. Gadbail, V. Joshi, Nitric oxide and cancer: a review, World J. Surgical Oncol. 11 (2013) 1–11.
[37] M.H. Mahnashi, Design, synthesis and biological screening of novel cucs inspired estrone analogues towards treatment of hepatocellular carcinoma, Chemistry and Biochemistry, South Dakota State University, South Dakota, 2017, p. 277.
[38] I.T. Schiefer, L. VandeVrede, M. Fa, O. Arancio, G.R.J. Thatcher, Furoxans (1,2,5-oxadiazole-N-oxides) as novel NO mimetic neuroprotective and procognitive agents, J. Med. Chem. 55 (2012) 3076–3087.
[39] A. Horton, K. Nash, E. Tackie-Yarboi, A. Kostrevski, A. Novak, A. Raghavan, J. Tulsulkar, Q. Alhadidi, N. Wamer, B. Langenderfer, K. Royster, M. Ducharme, K. Hagood, M. Post, Z.A. Shah, I.T. Schiefer, Furoxans (oxadiazole-4*N*-oxides) with attenuated reactivity are neuroprotective, cross the blood brain barrier, and improve passive avoidance memory, J. Med. Chem. 61 (2018) 4593–4607.
[40] Y. Liu, S.K. Park, Y. Xiao, J. Chae, Copper(II)-catalyzed C-O coupling of aryl bromides with aliphatic diols: Synthesis of ethers, phenols, and benzo-fused cyclic ethers, Organic Biomol. Chem. 12 (2014) 4747–4753.
[41] T. Ostlund, F. Halaweish, K. Alseud, In silico drug design of heterocyclic cucurbitacin- inspired estrone analogs targeting EGFR in lung cancer, Abstracts, 52nd Midwest Regional Meeting of the American Chemical Society, Lawrence, KS, United States, October 18–20, 2017, MWRM-100.
[42] W. Zhou, Y. Peng, S.-S. Li, Semi-synthesis and anti-tumor activity of 5,8-*O*-dimethyl acylshikonin derivatives, Eur. J. Med. Chem. 45 (2010) 6005–6011.
[43] M.-M. Liu, X.-Y. Chen, Y.-Q. Huang, P. Feng, Y.-L. Guo, G. Yang, Y. Chen, Hybrids of phenylsulfonylfuroxan and coumarin as potent antitumor agents, J. Med. Chem. 57 (2014) 9343–9356.
[44] F.F. El-Senduny, F.A. Badria, A.M. El-Waseef, S.C. Chauhan, F. Halaweish, Approach for chemosensitization of cisplatin-resistant ovarian cancer by cucurbitacin B, Tumor Biol. 37 (2016) 685–698.
[45] G. Ghosh, X. Lian, S.J. Kron, S.P. Palecek, Properties of resistant cells generated from lung cancer cell lines treated with EGFR inhibitors, BMC Cancer 12 (2012) 95.
[46] Z. Li, Y. Wang, C. Fu, X. Wang, J.J. Wang, Y. Zhang, D. Zhou, Y. Zhao, L. Luo, H. Ma, W. Lu, J. Zheng, X. Zhang, Design, synthesis, and structure-activity-relationship of a novel series of CXCR4 antagonists, Eur. J. Med. Chem. 149 (2018) 30–44.
[47] A.C. Pippione, I.M. Carnovale, D. Bonanni, M. Sini, P. Goyal, E. Marini, K. Pors, S. Adinolfi, D. Zonari, C. Festuccia, W.Y. Wahlgren, R. Friemann, R. Bagnati, D. Boschi, S. Oliaro-Bosso, M.L. Lolli, Potent and selective aldo-keto reductase 1C3 (AKR1C3) inhibitors based on the benzoisoxazole moiety: application of a bioisosteric scaffold hopping approach to flufenamic acid, Eur. J. Med. Chem. 150 (2018) 930–945.
[48] G. Caron, G. Ermondi, R.A. Scherrer, Lipophilicity, polarity, and hydrophobicity, in: J.B. Taylor, D.J. Triggle (Eds.), Comprehensive Medicinal Chemistry II, Elsevier, Oxford, 2007, pp. 425–452.
[49] M. Studenovsky, L. Sivak, O. Sedlacek, R. Konefal, V. Horkova, T. Etrych, M. Kovar, B. Rihova, M. Sirova, Polymer nitric oxide donors potentiate the treatment of experimental solid tumours by increasing drug accumulation in the tumour tissue, J. Control. Release 269 (2018) 214–224.
[50] S.Y. Hong, G.L. Borchert, A.E. Maciag, R.S. Nandurdikar, J.E. Saavedra, L.K. Keefer, J.M. Phang, H. Chakrapani, The nitric oxide prodrug V-PROLI/NO inhibits cellular uptake of proline, ACS Med. Chem. Lett. 1 (2010) 386–389.
[51] A.E. Maciag, R.J. Holland, Y.S. Robert Cheng, L.G. Rodriguez, J.E. Saavedra, L.M. Anderson, L.K. Keefer, Nitric oxide-releasing prodrug triggers cancer cell death through deregulation of cellular redox balance, Redox Biol. 1 (2013) 115–124.
[52] X. Li, X. Wang, C. Xu, J. Huang, C. Wang, X. Wang, L. He, Y. Ling, Synthesis and biological evaluation of nitric oxide-releasing hybrids from gemcitabine and phenylsulfonyl furoxans as anti-tumor agents, MedChemComm 6 (2015) 1130–1136.
[53] LI-COR, Western blot and in-cell western™ assay detection using IRDye® subclass specific antibodies. https://www.licor.com/documents/86xilzixljcaz6rreqy9fx8dwz4rps55, 2011 (accessed March 2011).
[54] L. Chen, Q. Li, B. Weng, J. Wang, Y. Zhou, D. Cheng, T. Sirirak, P. Qiu, J. Wu, Design, synthesis, anti-lung cancer activity, and chemosensitization of tumor-selective MCACs based on ROS-mediated JNK pathway activation and NF-κB pathway inhibition, Eur. J. Med. Chem. 151 (2018) 508–519.
[55] Y. Fang, W. Xia, B. Cheng, P. Hua, H. Zhou, Q. Gu, J. Xu, Design, synthesis, and biological evaluation of compounds with a new scaffold as anti-neuroinflammatory agents for the treatment of Alzheimer's disease, Eur. J. Med. Chem. 149 (2018) 129–138.
[56] Cell Signaling Technology, In-cell western protocol. https://www.cellsignal.com/contents/resources-protocols/in-cell-western-protocol/in-cell-western-protocol, 2010 (accessed June 2010).
[57] ROCKLANDTM antibodies and assays, In-cell western protocol. https://rockland-inc.com/uploadedFiles/Support/Protocols/In_cell_Western_Protocol_v3.pdf.
[58] Y.L. Sun, A. Patel, P. Kumar, Z.S. Chen, Role of ABC transporters in cancer chemotherapy, Chinese J. Cancer 31 (2012) 51–57.
[59] T.-C. Lee, I.-C. Ho, W.-J. Lu, J.-D. Huang, Enhanced expression of multidrug resistance-associated protein 2 and reduced expression of aquaglyceroporin 3 in an arsenic-resistant human cell line, J. Biol. Chem. 281 (2006) 18401–18407.

[60] C.S. Morrow, P.K. Smitherman, A.J. Townsend, Role of multidrug-resistance protein 2 in glutathione S-transferase P1-1-mediated resistance to 4-nitroquinoline 1-oxide toxicities in HepG2 cells, Mol. Carcinog. 29 (2000) 170–178.
[61] M.S. Ahmed, L.C. Kopel, F.T. Halaweish, Structural optimization and biological screening of a steroidal scaffold possessing cucurbitacin-like functionalities as B-Raf inhibitors, ChemMedChem 9 (2014) 1361–1367.
[62] S.G. Abdel Moty, M.A. Hussein, S.A. Abdel Aziz, M.A. Abou-Salim, Design and synthesis of some substituted thiazolo[3,2-a]pyrimidine derivatives of potential biological activities, Saudi Pharm. J. 24 (2016) 119–132.
[63] N.-J. Fan, Y.-Y. Han, Y.-F. Li, J.-M. Gao, J.-J. Tang, Synthesis of novel 4′-acylamino modified 21E-benzylidene steroidal derivatives and their cytotoxic activities, Steroids 123 (2017) 20–26.
[64] N.-J. Fan, Y.-B. Bai, F.-Y. Zhang, B. Luo, J.-J. Tang, Q.-Z. Zhang, J.-M. Gao, Synthesis and cytotoxicity of some novel 21E-benzylidene steroidal derivatives, Steroids 78 (2013) 874–879.
[65] L. Troisi, S. Florio, C. Granito, Chemoselective construction of novel steroid derivatives, Steroids 67 (2002) 687–693.
[66] T. Fujihara, K. Semba, J. Terao, Y. Tsuji, Copper-catalyzed hydrosilylation with a bowl-shaped phosphane ligand: preferential reduction of a bulky ketone in the presence of an aldehyde, Angew. Chem. Int. Ed. 49 (2010) 1472–1476.
[67] Y. Tamboli, L. Lazzarato, E. Marini, S. Guglielmo, M. Novelli, P. Beffy, P. Masiello, R. Fruttero, A. Gasco, Synthesis and preliminary biological profile of new NO-donor tolbutamide analogues, Bioorganic Med. Chem. Lett. 22 (2012) 3810–3815.
[68] K. Chegaev, L. Lazzarato, G.C. Tron, D. Marabello, A.D. Stilo, C. Cena, R. Fruttero, A. Gasco, N. Vanthuyne, C. Roussel, Synthesis, chiral HPLC resolution and configuration assignment of 1-phenylglyceryl trinitrate stereomers, Chirality 18 (2006) 430–436.
[69] A. Huether, M. Höpfner, A.P. Sutter, D. Schuppan, H. Scherübl, Erlotinib induces cell cycle arrest and apoptosis in hepatocellular cancer cells and enhances chemosensitivity towards cytostatics, J. Hepatol. 43 (2005) 661–669.
[70] F.A. Mohammed, A.I. Elkady, F.Q. Syed, M.B. Mirza, K.R. Hakeem, S. Alkarim, Anethum graveolens (dill) – a medicinal herb induces apoptosis and cell cycle arrest in HepG2 cell line, J. Ethnopharmacol. 219 (2018) 15–22.
[71] OpenEye Scientific Software, Fast Rigid Exhaustive Docking (FRED) Receptor, version 2.2.5 http://www.eyesopen.com, 2018 (accessed 2018).
[72] OpenEye Scientific Software, FRED, version 2.2.3. http://www.eyesopen.com, 2018 (accessed 2018).
[73] OpenEye Scientific Software, VIDA, version 4.1.2. http://www.eyesopen.com, 2018 (accessed 2018).
[74] Molinspiration, Calculation of molecular properties and bioactivity score. http://www.molinspiration.com/cgi-bin/properties, 2018 (accessed 2018).